

MICROEMULSION-MEDIATED SYNTHESIS OF NANOSIZE MOLYBDENUM SULFIDE COAL LIQUEFACTION CATALYSTS

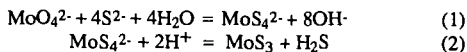
E. Boakye, N. Vaidyanathan, L.R. Radovic and K. Osseo-Asare
Department of Materials Science and Engineering
The Pennsylvania State University, University Park, PA 16802

INTRODUCTION

In heterogeneous catalysis, the size of the catalyst is of considerable importance in that the extent of reaction is often inversely proportional to the particle size of the catalyst. As a consequence, various methods have been used to synthesize particles of large specific surface area for catalysis applications (1-3). Most of these methods are based on hydrocolloids (1) and aerosols (2). Recently microemulsion-based synthesis is also attracting attention (3). Haruta et al. (1) prepared molybdenum sulfide particles in the micrometer size range by reacting ammonium molybdate and thioacetamide. Different particle sizes were obtained by varying the pH. In the preparation of iron sulfide catalysts for coal liquefaction, Andres et al. (2) used an aerosol-based method to synthesize iron oxide particles which were used *in situ* with carbon disulfide to liquefy coal. The liquefaction yield was found to be inversely proportional to the particle size. The synthesis of nanosize particles using inverse microemulsions has been reported for a variety of materials (4,5), among which are the hydrogenation catalysts nickel and cobalt borides (3), and platinum-group metals (6,7). Others worth noting are cadmium sulfide (4,8-10), copper, lead, and indium sulfides (9,11), cadmium selenide (12), silica (5), and silver halide (13,14). In this communication a microemulsion-based method for the synthesis of molybdenum sulfide nanosize particles is reported for the first time. This material is currently under active investigation as a potential coal liquefaction catalyst (15).

An inverse microemulsion is a thermodynamically stable, optically isotropic dispersion of microdrops of water in an external oil phase stabilized by a surfactant (16-18). The microemulsion systems used in this study are: polyoxyethylene(5)nonylphenylether (NP-5)/cyclohexane/water and NP-5/tetralin/benzyl alcohol/water. The latter system was used previously in this laboratory as a medium for the synthesis of silica nanoparticles (5). In these systems the water molecules interact with the hydrophilic portion of the surfactant molecules via hydrogen bonding to form inverse micelles. The addition of more water molecules results in the formation of swollen inverse micelles, often referred to as inverse microemulsions. The water pools inside the inverse micelles vary in size depending on the water-to-surfactant molar ratio (R) and are in the size range of 3-30 nm (16-18). Due to the cage-like nature of the water pools, particle growth is limited when particle precipitation is effected in them. Advantage has been taken of this unique property of inverse microemulsions to synthesize nanosize molybdenum sulfide particles in the size range 10-150 nm. The large surface area available on these nanoparticles results in a high yield of hexane-soluble oils when coal is liquefied (15).

The chemistry pertaining to the formation of molybdenum sulfide is summarized below:



The following thiomolybdate species are formed when ammonium molybdate is reacted with the sulfide ligand at a pH of 3-11: $\text{MoO}_3\text{S}^{2-}$, $\text{MoO}_2\text{S}_2^{2-}$, MoOS_3^{2-} and MoS_4^{2-} . Extensive formation of the tetrathiomolybdate ion depends on the sulfur-to-molybdenum ratio and on solution pH (19-22). As can be seen from Equation 2, molybdenum sulfide forms when an acid is added to tetrathiomolybdate species.

EXPERIMENTAL SECTION

The following chemicals were obtained from Aldrich: the non-ionic surfactant polyoxyethylene(5)nonylphenylether (NP-5), ammonium tetrathiomolybdate (99.97%), cyclohexane (99%) and 1,2,3,4-tetrahydronaphthalene (tetralin). Before use cyclohexane and tetralin were dried with molecular sieves. The inverse microemulsions NP-5/cyclohexane/water and NP-5/tetralin/benzyl alcohol/water were prepared at room temperature by adding 10% sulfuric acid to a solution of 0.134 M NP-5/cyclohexane and 0.4 M NP-5/tetralin/benzyl alcohol, respectively. The acid-solubilized microemulsion was deoxygenated by bubbling nitrogen gas through it for 20 min. This procedure was followed by adding 1×10^{-3} M and 1×10^{-2} M ammonium tetrathiomolybdate to the 0.134 M NP-5/cyclohexane and 0.4 M NP-5/tetralin/benzyl alcohol, respectively. Nitrogen was further bubbled while the molybdenum sulfide was being precipitated according to Equation 2. For the NP-5/cyclohexane/water microemulsion the concentration of the reactant species was constant with respect to the total microemulsion. On the other hand, in the case of the NP-5/tetralin/benzyl alcohol/water microemulsion, the concentration of the reactant species was maintained at a constant value with respect to the water pools.

Ultraviolet/visible spectra were obtained with a Hewlett Packard 84151A diode array spectrophotometer. Samples for transmission electron microscopy were prepared by directly dropping a very small amount of molybdenum sulfide dispersion on carbon-coated copper grids and drying at room temperature. Prior to sample extraction, each sample bottle was sonicated for 1 min. Particle sizes were determined with a Philips 420 transmission electron microscope operating at 120 kV with a resolution of about 0.6 nm. The diameters of at least 300 particles were measured for each sample to obtain an average particle diameter and standard deviation.

RESULTS AND DISCUSSION

Molybdenum sulfide nanoparticles have been synthesized successfully in the following microemulsion systems: NP-5/cyclohexane/water and NP-5/tetralin/benzyl alcohol/water. Figures 1 and 2, respectively, refer to the ultraviolet/visible absorption spectra of ammonium tetrathiomolybdate and molybdenum sulfide particles in a 0.1 M NP-5/cyclohexane microemulsion system. The microemulsions represented in these two figures contained equal amounts of 1.0×10^{-3} M ammonium tetrathiomolybdate, except that the microemulsion in Figure 2 contained 10% sulfuric acid. These two figures are different in that the absorption peaks for MoS_4^{2-} and $\text{MoO}_2\text{S}_2^{2-}$ (23) are absent in Figure 2 while a peak with an onset wavelength of about 350 nm appears. The disappearance of the peaks for the thiomolybdate species suggests that conversion (i.e., Equations 2 and 3) took place in the inverse microemulsion when the thiomolybdate species found themselves in the same inverse micelle with protons:



NP-5/Cyclohexane/Water. Figures 3 and 4, respectively, present TEM micrographs of molybdenum sulfide particles in the 0.134 M NP-5/cyclohexane/water microemulsion system and a plot of water-to-surfactant molar ratio (R) versus the average particle diameter. The average particle diameter decreases with R to a value of 2 and then increases with R. This trend may be rationalized in terms of nucleation and growth phenomena (3,4,14). The process of particle formation from dissolved ions can be represented in the following order: Ions \rightarrow Monomer \rightarrow Nuclei \rightarrow Particles (24). After a stable nucleus is formed, it can grow by the following growth processes: (a) Incorporation of ions and monomers in solution into already formed nuclei (3), and (b) aggregation of primary particles or nuclei to form bigger particles (4,14).

The nucleation and initial growth of particles takes place in the inverse micelles through collision, fusion and splitting of inverse micelles. In order to form a stable nucleus, a cluster containing a critical number of monomers (N_c) must form. A useful

parameter in this connection is that of the ion occupancy number, i.e., the number of reactant species in an inverse micelle. A nucleus is formed if the ion occupancy number is greater than N_c . As the water-to-surfactant molar ratio is decreased, the surfactant aggregation number decreases (25,26) and the micellar concentration increases. This corresponds to a decrease in the ion occupancy number because the concentrations of the reactant species (MoS_4^{2-} and H^+) in the microemulsion are constant. For low R values, relatively fewer water cores will therefore contain the minimum number of ions required to form a nucleus. As a result, the ions left over after the nucleation process are relatively large. These ions will be incorporated into the already formed nuclei via inter- and intramicellar communication and will contribute to growth, leading to large particles, as demonstrated by the top left side of Figure 4.

As R increases, the aggregation number increases, the micellar concentration decreases, and therefore the ion occupancy number increases. The observed decrease in particle size with increase in R below $R=2$ can be attributed to the increase in ion occupancy number with R. From nucleation theory, the greater the number of nuclei in the inverse microemulsion, the smaller the particle size. This is because there will be relatively few ions left over after the nucleation process, i.e., almost all the ions are used up in the nucleation process.

At $R>2$ the proportion of water in the microemulsion is relatively large, hence the aggregation number is large and the concentration of swollen inverse micelles (water pools) is significantly reduced. As a first approximation, if only one nucleus forms in a water pool, then the decrease in the number of water pools corresponds to a decrease in the number of nuclei that transform into primary particles; hence, there is an increase in the concentration of excess ions which are not utilized in the nuclei formation and are therefore available for particle growth.

NP-5/Tetralin/Benzyl Alcohol/Water. The microemulsion system consisting of NP-5/tetralin/benzyl alcohol has an inherent advantage for coal liquefaction in that tetralin is an excellent process solvent and hence the need to harvest the particles from the synthetic medium can be avoided. Figures 5 and 6 represent respectively the TEM micrograph and a plot of the average particle size versus the water-to-surfactant molar ratio (R) in the 0.4 M NP-5/tetralin/benzyl alcohol/water microemulsion. The particle size decreases with increasing R to a value of 2, and then increases with R. The trend in Figure 6 can be explained in an analogous manner to that observed in Figure 4. In this system two factors, i.e., the water-to-surfactant molar ratio (R) and reactant concentration, increased the ion occupancy number simultaneously.

CONCLUSIONS

Nanosize molybdenum sulfide particles have been synthesized in 0.134 M NP-5/cyclohexane/water and 0.4 M NP-5/tetralin/benzyl alcohol/water microemulsions. The particle size varies with the water-to-surfactant molar ratio. The synthesis of molybdenum sulfide using tetralin as a solvent has potentially important technological applications since catalyst preparation does not involve particle harvesting. Advantage can be taken of the variation of particle size with the water-to-surfactant molar ratio (R) to make particles of desired sizes for coal liquefaction. It should be mentioned that liquefaction tests conducted so far have given high yields of hexane-soluble oils and the yield of oils has been found to be inversely proportional to particle size (15).

ACKNOWLEDGEMENT

This work is being supported by the Department of Energy, Contract No. DE-AC22-90PC90054.

REFERENCES

1. M. Haruta, J. Lemaitre, F. Delannay and B. Delmon, *J. Coll. Interf. Sci.* **101**, 59 (1984).
2. M. Andres, H. Charcosset, P. Chiche, L. Davignon, G. Djega-Mariadassou, J.P. Joly and S. Pregermain, *Fuel* **62**, 69 (1983).
3. I. Ravet, J.B. Nagy and E.G. Derouane, in "Preparation of Catalysts IV," Elsevier (B. Delmon, P. Grange, P.A. Jacobs and G. Poncelet, Eds.), 1987, p. 505.
4. T.I. Towey, A. Khan-Lodhi and B.H. Robinson, *J. Chem Soc. Faraday Trans.* **86**, 3757 (1990).
5. K. Osseo-Asare and F.J. Arriagada, *Coll. Surf.* **50**, 321 (1990).
6. M. Boutonnet, J. Kizling and P. Stenius, *Coll. Surf.* **5**, 209 (1982).
7. A. Claerbout and J.B. Nagy, in "Preparation of Catalysts V," Elsevier (G. Poncelet, P.A. Jacobs, P. Grange and B. Delmon, Eds.), 1991, p. 705.
8. C. Petit and M.P. Pileni, *J. Phys. Chem.* **98**, 2282 (1988).
9. P. Lianos and J.K. Thomas, *Mater. Sci. Forum* **25-26**, 369 (1988).
10. S. Modes and P. Lianos, *J. Phys. Chem.* **93**, 5854 (1989).
11. T. Dannhausser, M. O'Neil, K. Johansson, D. Whitten and G. McLendon, *J. Phys. Chem.* **90**, 6074 (1986).
12. M.L. Steingerwald, A.P. Alivisatos, J.M. Gibson, T.D. Harris, R. Kortan, A.J. Muller, A.M. Thayer, T.M. Duncan, D.C. Douglas and L.E. Brus, *J. Am. Chem. Soc.* **110**, 3046 (1988).
13. M. Dvolaitzky, R. Ober, C. Taupin, R. Anthore, X. Auvray, C. Petipas and C. Williams, *J. Dispers. Sci. Technol.* **4**, 29 (1988).
14. M.I. Hou and D.O. Shah, in "Interfacial Phenomena in Biotechnology and Materials Processing" (Y. Attia, B.M. Moudhil and S. Chander, Eds.), Elsevier, 1988, p. 443.
15. N. Vaidyanathan, E. Boakye, K. Osseo-Asare and L.R. Radovic, *ACS Preprints, Fuel Chem. Div.* (San Francisco, 1992), in press.
16. J.H. Fendler, *Chem. Rev.* **87**, 877 (1987).
17. B. Lindman, P. Stilbs and M.E. Moseley, *J. Coll. Interf. Sci.* **83**, 569 (1981).
18. S.E. Friberg and P. Bothorel (Eds.), *Microemulsions: Structure and Dynamics*, CRC Press (Boca Raton, FL), 1987.
19. J. Prasilova and J. Burclova, *Radiochem. Radioanal. Lett.* **11**, 351 (1972).
20. V. Yatirajam, U. Ahuja and L.R. Kakkur, *Talanta* **23**, 819 (1976).
21. N.J. Clarke and S.H. Laurie, *J. Inorg. Biochem.* **12**, 37 (1980).
22. M.A. Hammer and A.G. Sykes, *Inorg. Chem.* **19**, 2881 (1980).
23. P.J. Aymonino, A.C. Ranade, E. Diemann and A. Muller, *Z. Anorg. Allgem. Chem.* **371**, 300 (1969).
24. A.E. Nielson, *Kinetics of Precipitation*, MacMillan, New York, 1964.
25. A. Veerbek, E. Gelade and F.C. De Schryver, *Langmuir* **2**, 448 (1986).
26. J.C. Railey and M. Buzier, *J. Coll. Interf. Sci.* **116**, 30 (1987).
27. J.B. Nagy, A. Gourgue and E.G. Derouane, *Stud. Surf. Sci. Catal.* **16**, 93 (1983).

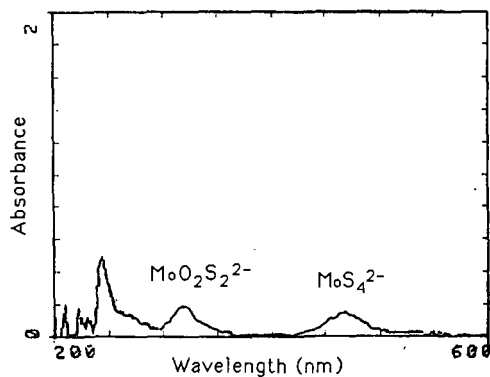


Figure 1. Absorption spectrum of 1×10^{-3} M thiomolybdate species in 0.1 M NP-5/cyclohexane/water microemulsion, $R=3$. (The concentration of the thiomolybdate species is with respect to the water pool volume.)

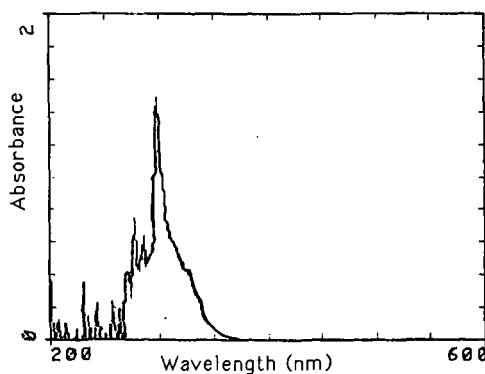


Figure 2. Absorption spectrum of molybdenum sulfide in 0.1 M NP-5/cyclohexane/water microemulsion, $R=6$, $[\text{MoS}_4^{2-}] = 1 \times 10^{-3}$ M. (The concentration of thiomolybdate species is with respect to the water pool volume.)

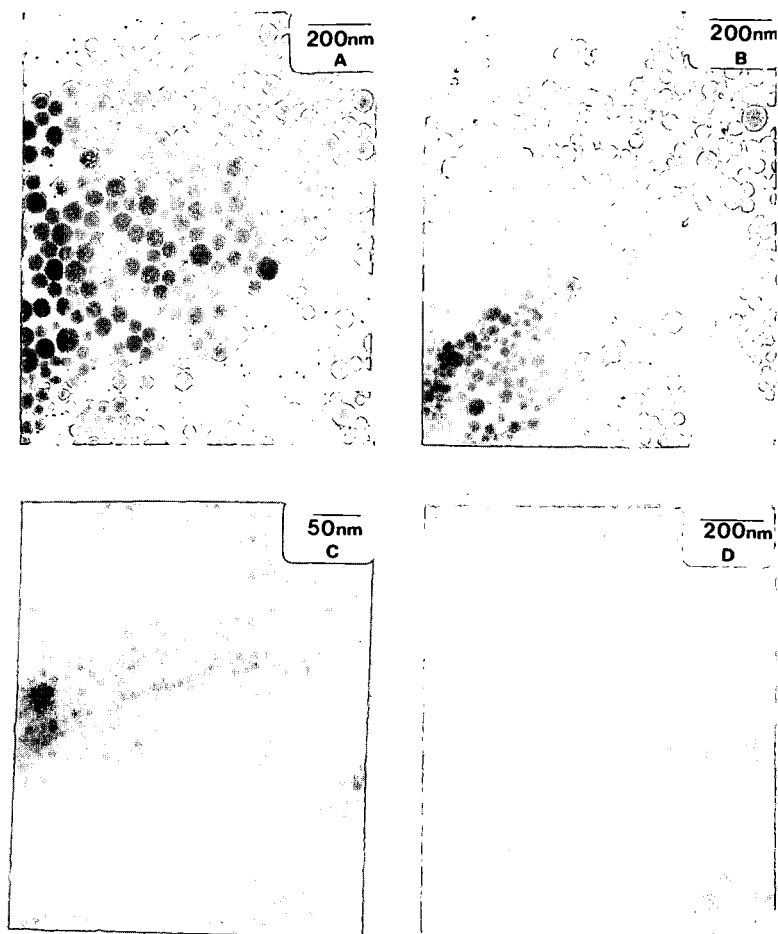


Figure 3. TEM micrographs of molybdenum sulfide particles prepared in 0.134 M NP-5/cyclohexane/water microemulsions: (A) R=1; (B) R=1.5; (C) R=2; (D) R=3.

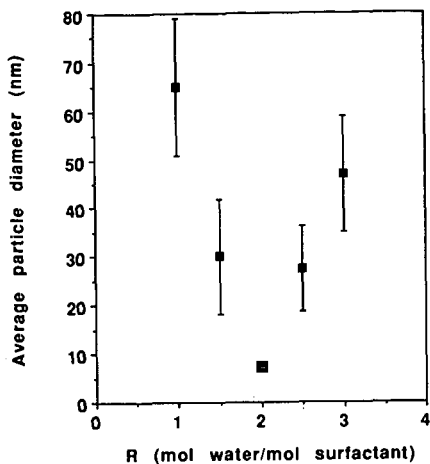


Figure 4. Effect of water-to-surfactant molar ratio (R) on average particle size for the 0.134 M NP-5/cyclohexane/water microemulsion. (The concentration of reactant species is constant with respect to the microemulsion.)

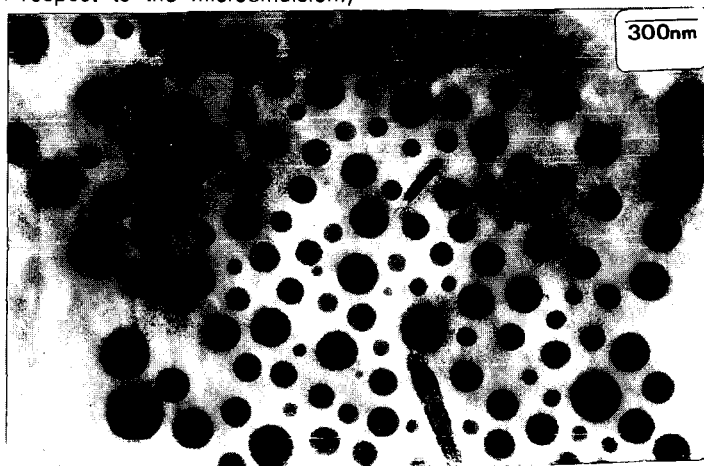


Figure 5. TEM micrograph of molybdenum sulfide prepared in 0.4 M NP-5/tetralin/benzyl alcohol microemulsion.

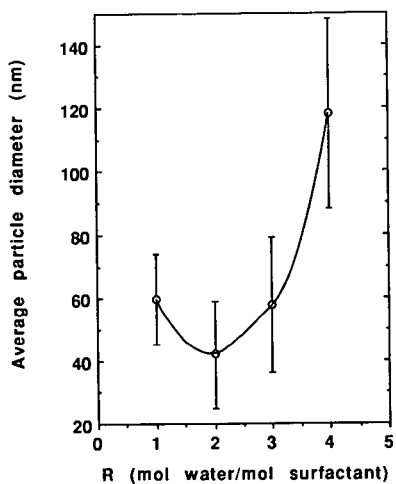


Figure 6. A plot of average particle diameter versus water-to-surfactant molar ratio (R) for the 0.4M NP-5/tetralin/benzyl alcohol microemulsion. The concentration of reactant species is constant with respect to the water pools.

IN-SITU MODEL STUDIES OF METAL SULFIDE CATALYSTS

N.M. Rodriguez, and R.T.K. Baker
Chemical Engineering Department,
Auburn University
Auburn, AL 36849

Keywords: In-situ Electron Microscopy, catalytic hydrogenation of graphite, metal sulfide-hydrogen interactions

ABSTRACT

In-situ electron microscopy studies of the dynamic behavior of certain metal sulfides supported on single crystal graphite showed that when such specimens were treated in 0.2 Torr hydrogen, pitting of the carbonaceous support at edges, steps and defect regions of the basal plane occurred. In the absence of a catalyst attack of graphite by molecular hydrogen was not observed until the temperature was raised to above 1000°C. In contrast, when a metal sulfide was present gasification of the graphite took place at very low temperatures. We believe that this unusual behavior, which is quite different to that observed in the presence of metal catalysts, is the result of attack by atomic hydrogen which is produced from the interaction of molecular hydrogen with the metal sulfide particles. These observations are consistent with those of other workers who have studied the interaction of microwave generated atomic hydrogen species with graphite.

INTRODUCTION

Over recent years a considerable wealth of knowledge has been amassed on the manner by which catalysts can modify both the rate and selectivity of various reactions involving the conversion of petroleum feedstocks into a variety of fuel fractions and chemicals. There are tremendous opportunities available if one can learn how to exploit the potential of these petroleum-related catalyst systems to manipulate the decomposition of coal to produce a similar spectrum of speciality chemicals. Of particular importance with regard to the conversion of carbonaceous solids such as coal to high molecular weight hydrocarbons are the catalytic reactions involving hydrogen. In this context, it is well worth considering the phenomenon of migration or "spillover" of adsorbed species which is known to occur with certain supported metal catalyst systems. Perhaps the most widely known example of spillover behavior is that associated with dissociation of molecular hydrogen over certain metal catalysts.

The phenomenon of hydrogen spillover was first suggested from the observations that the rate of decomposition of GeH₄ to Ge was accelerated in the presence of platinum¹. The effect was also demonstrated by very elegant experiments in which the transformation of WO₃ to H_xWO₃ during treatment in hydrogen in the presence of Pt/Al₂O₃ induced a color change from yellow to blue². Hydrogen spillover also appears to play an important role in the extent of reduction of a titanium oxide support when platinum was introduced onto this material and the system heated in hydrogen^{3,4}. Early work by Boudart and coworkers⁵ showed that hydrogen spillover from platinum to carbon occurred at 350°C and subsequently it has been demonstrated that this behavior can lead to methanation of the solid carbon⁶⁻⁸. Although the nature of the diffusing species is not yet established, it does appear that atomic hydrogen could be involved in the reaction mechanism.

The concept of using atomic hydrogen to convert carbonaceous solids to an assortment of hydrocarbon products has been reported by a number of workers⁹⁻¹⁸. In these studies hydrogen atoms were generated either in low pressure microwave discharge systems or by dissociation of molecular hydrogen over a hot tungsten filament. There is general agreement that the interaction of atomic hydrogen with carbonaceous solids can take place at a relatively rapid rate even at room temperature. On the other hand, a wide variation in the hydrocarbon product distribution and composition has been reported from such reactions, which appears to be related to the type of discharge system used to produce atomic hydrogen, the hydrogen pressure and the time of exposure. Vastola and coworkers¹¹ and later Gesser and Czubryl¹⁸ found that acetylene and methane were the major products with minor amounts of ethane, methylacetylene and pentane arising from the reaction of atomic hydrogen with graphite. In another study, Gill and coworkers¹⁰ produced hydrogen atoms by dissociation of H₂ over a tungsten filament and allowed these atoms to react with a carbon solid at 77K. At low pressure conditions methane, ethane, propane and butene along with an identified higher molecular weight compound were produced from the reaction with graphite. In contrast only methane and ethane were formed at higher pressures when helium was added to the hydrogen.

From this brief overview of the interaction of atomic hydrogen species with coals and carbons it is clear that this approach holds a great deal of potential for the conversion of such solids into a variety of extremely useful precursor hydrocarbon molecules. The notion of producing atomic hydrogen via various discharge techniques is extremely interesting and offers the opportunity of controlling the energy of the atomic species, however, this experimental approach is fraught with technical difficulties when one attempts to scale up such a reactor system. The question which arises is can we perform such reactions by generating atomic hydrogen species from a somewhat simpler route, i.e. by catalytic dissociation of molecular hydrogen.

The characteristics of a suitable candidate for this operation would be one which has the capacity to dissociate molecular hydrogen in a reversible manner at relatively low temperatures. Examination of the literature shows that while the majority of metals are capable of dissociating molecular hydrogen, they do not readily release the atomic species. In contrast, it appears that certain metal sulfides and in particular molybdenum disulfide may well possess the desired characteristics¹⁹.

In the current study we have used the technique of controlled atmosphere electron microscopy to directly observe the behavior of hydrogen on two types of model catalyst systems:

- (a) cobalt supported on graphite, and,
- (b) molybdenum disulfide on graphite.

These two catalyst systems were found to exhibit dramatic differences in their behavior towards hydrogen and reasons for these observations are discussed.

EXPERIMENTAL

The experiments reported here were performed using a modified JEOL 200CX TEM electron microscope. This instrument is equipped with a custom designed environmental cell, which accommodates a heating stage. Specimens can be heated

up to a temperature of 1000°C while at the same time being exposed to a gas environment at pressures up to 3.0 Torr. The resolution of this instrument when used in conjunction with a closed-circuit television system is of the order of 0.4 nm.

Transmission specimens of single crystal graphite and molybdenum disulfide were prepared by a standard cleaving technique. Two procedures were used to prepare molybdenum disulfide/graphite specimens. In the first method, the sulfide was introduced onto the graphite in the form of particles from an ultrasonic dispersion of the powder in iso-butanol. In a second approach, transmission sections of both materials were mounted side by side on nickel grids. Cobalt was deposited onto the graphite substrates by evaporation of spectrographically pure wire from a tungsten filament at a residual pressure of 10^{-6} Torr. The conditions were selected so as to produce a film of metal at least one atom on average thickness. The reactant gas, hydrogen, was 99.999 % pure and used without further purification.

RESULTS AND DISCUSSION

(a) Cobalt/Graphite - Hydrogen

When cobalt/graphite specimens were heated in the presence of 0.2 Torr hydrogen, the deposited metal film was observed to nucleate into discreet particles at 350°C. On continued heating particles located on the graphite edge and steps sites were seen to exhibit dramatic changes in their wetting characteristics with the substrate and this behavior was reflected in a change in the mode by which they operated during the subsequent hydro-gasification reaction. This sequence of events is depicted schematically in Figure 1. At 400°C, particles were found to undergo a wetting and spreading action along the graphite prismatic faces. This behavior preceded the onset of catalytic attack at 450°C, which took place by the edge recession mode. It was interesting to find that the receding edges were aligned in particular directions, being parallel to the $\langle 11\bar{2}0 \rangle$ crystallographic orientations of graphite.

At 650°C, the catalyst exhibited a modification in its wetting properties with the graphite, which resulted in the re-formation of particles. This transformation was accompanied by a change in the mode of catalytic attack from edge recession to channeling. During channeling the active particles maintain contact with the graphite interface and as a consequence during propagation across the basal plane, always remain at the leading face of the channel. Quantitative kinetic measurements of a number of channeling sequences showed that the typical propagation rates exhibited by 25 nm diameter particles at 840°C was of the order of 10 nm/sec. A survey of many regions of the specimen revealed that the majority of channels were straight and oriented parallel to the $\langle 11\bar{2}0 \rangle$ graphite crystallographic directions.

It is possible that the observed a change in wetting characteristics of the metal particles on the graphite which takes place at 650°C is a result of carbon being dissolved in the metal particles, and this event is known to induce changes in the interfacial energy of such particles²⁰. Previous studies with other metals have shown that although this behavior appears to be a general phenomenon²¹, the temperature where such transformations occur vary with each system. Finally, it is clear that in this type of catalyzed hydro-gasification reaction the removal of carbon atoms to form methane only occurs at the catalyst/graphite interface, there being no evidence for loss of carbon from regions devoid of catalyst material at temperatures below 1000°C.

(b) Molybdenum Disulfide/Graphite - Hydrogen

Treatment of graphite specimens containing particulates of molybdenum disulfide, in 0.2 Torr hydrogen produced some very unusual effects. Inspection of the graphite surface showed that even at room temperature erosion of certain regions of the basal plane was taking place. This took the form of the creation of very tiny pits (~ 3 nm width), which initially tended to form as discreet clusters. On continued reaction at the same temperature these pits expanded along certain directions and developed into single larger pits, about 10 nm in width, which adopted an hexagonal outline with an internal island of carbon. This sequence of events is shown in the schematic diagram, Figure 2. As the reaction proceeded it became apparent that the formation of pits was not restricted to regions in the immediate vicinity of the sulfide particles. Indeed, they tended to preferentially occur at surface imperfections on the graphite basal plane such as vacancies, steps and along twin bands. Other workers^{22,23} have used the gold decoration technique to demonstrate that atomic hydrogen species can attack the basal plane regions of graphite to produce monolayer pits. Such features would not be observed in the present experiment since the contrast difference afforded by conventional TEM does not allow one to distinguish differences in thickness down to this level.

It is difficult to rationalize these extraordinary observations without invoking the participation of very reactive species such as atomic hydrogen which is produced by dissociation of molecular hydrogen on the sulfide catalyst. The pattern of behavior found in this work is consistent with that reported by other workers who have studied the interaction of microwave generated atomic hydrogen species with graphite. The finding that attack of the graphite surface could take place at regions remote from the catalyst particles suggests that the active entities have the ability to migrate across the graphite surface to active sites via a "spillover" mechanism. Initial concern that the electron beam might be exerting some influence on the reaction was dispelled in subsequent experiments by performing blank experiments in which specimens were reacted in hydrogen in the absence of the beam for periods of up to 2 hours. When such specimens were eventually examined it was clear that there had been extensive reaction prior to exposure to the beam.

On raising the temperature to 100°C the attack became indiscriminate in nature so that the whole surface gradually acquired a textured appearance. Also at this time, it was evident that the initially formed pits were tending to lose their faceted outline and become more circular in shape reaching diameters of 40 nm. In many cases, as pits expanded they merged into adjacent ones with a result that vast areas of the graphite surface were progressively removed.

The intensity of the reaction increased perceptibly at 200°C and it was significant to find that over prolonged periods at this temperature a carbonaceous deposit started to accumulate on the surface with the result that in some cases it was difficult to resolve the presence of shallow pits that had been previously apparent at lower temperatures. This observation suggests the possibility that some of the graphite is undergoing hydrogasification to produce hydrocarbons other than methane, which are susceptible to decomposition in the presence of the electron beam. At 350°C the reaction became so extensive that under these conditions the surface acquired a holey structure and experiments were normally terminated as the graphite specimens gradually lost their integrity.

In a further series of experiments the form of the specimen was changed to that where the molybdenum disulfide and graphite components were physically separated from one another. When this combination was reacted in 0.2 Torr hydrogen then attack of the pristine graphite surface was once again observed at room temperature. The subsequent behavior of these specimens was identical to that described above. The finding that it is not necessary for the catalyst to be in direct contact with the carbonaceous solid in order to promote hydro-gasification suggests that at the gas pressures used in these experiments it is possible for the active species to be transported through the gas phase in addition to the surface migration route.

ACKNOWLEDGMENTS

Financial work for this research was provided by the United States Department of Energy, Basic Energy Sciences, Grant DE-FG05-89ER14076 and CFFLS program Contract No DE-FC22-90-PC90029

REFERENCES

1. Taylor, H. S., *Ann. Rev. Phys. Chem.*, **5**, 646 (1967).
2. Khoobiar, S., *J. Phys. Chem.* **68**, 411 (1964).
3. Baker, R. T. K., Prestridge, E. B., and Murrel, L. L., *J. Catal.* **79**, 348 (1983).
4. Dumesic, J. A., Stevenson, S. A., Sherwood, R. D., and Baker, R. T. K., *J. Catal.* **99**, 79 (1986).
5. Boudart, M., Aldag, A. W., and Vannice, M. A., *J. Catal.* **18**, 46 (1970).
6. Tomita, A., and Tamai, Y., *J. Catal.* **27**, 293 (1972).
7. Olander, D. R. and Balooch, M., *J. Catal.* **60**, 41 (1979).
8. Chang, T. S., Rodriguez, N. M., and Baker, R. T. K., *J. Catal.* **123**, 486 (1990).
9. Blackwood, J. D., and McTaggart, F. K., *Aust. J. Chem.*, **12**, 533 (1959).
10. Gill, P. S., Toomey, R. E., and Moser, H. C., *Carbon* **5**, 43 (1967).
11. Vastola, F. J., Walker, Jr., P. L. and Wightman, J. P., *Carbon* **1**, 11 (1963)
12. Wood, B. J., and Wise, H., *J. Phys. Chem.* **73**, 1348 (1969)
13. McCarroll, B., and McKee, D. W., *Carbon*, **9**, 301 (1971)
14. Sanada, Y., and Berkowitz, N., *Fuel*, **48**, 375 (1969).
15. Amano, A., Yamada, M., Shindo, T., and Akakura, T., *Fuel* **63**, 718 (1984).
16. Amano, A., Yamada, M., Shindo, T., and Akakura, T., *Fuel* **64**, 123 (1985).
17. Wong, C.-L. Chen, C.-W. and Timmons, R. B., *Fuel* **65**, 1483 (1986).
18. Gesser, H. D., and Czubryt, J. J., *Fuel* **67**, 375 (1988).
19. Wright, C. J., Sampson, C., Fraser, D., Moyes, R. B., Wells, P. B. and Riekel, C., *J.C.S. Faraday I* **76**, 1585 (1980).
20. Weisweiler, W., and Mahadevan, V., *High Temp.-High Pressures* **4**, 27 (1972).
21. Baker, R. T. K., in "Carbon and Coal Gasification" (Eds. Figueiredo, J. L., and Mouljn, J. A.) Martinus Nijhoff Publishers, The Netherlands, 231 (1986).
22. Chen, J. P. and Yang, R. T., *Surf. Sci.* **216**, 481 (1989).
23. Pan, Z. J., and Yang, R. T., *J. Catal.* **123**, 206 (1990).

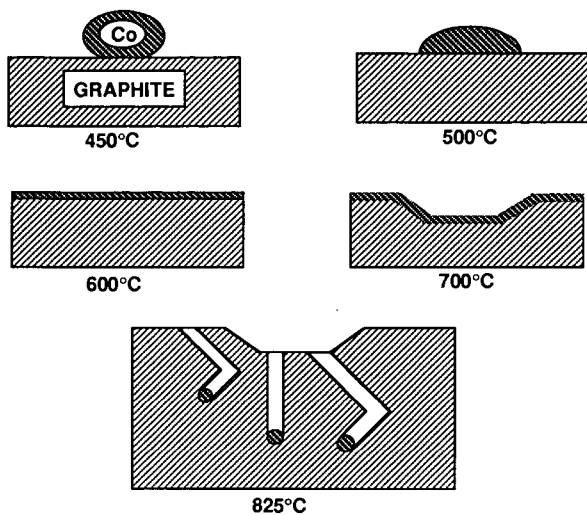


FIGURE 1. Change in wetting properties of a particle on graphite and the concomitant modification in catalytic action.

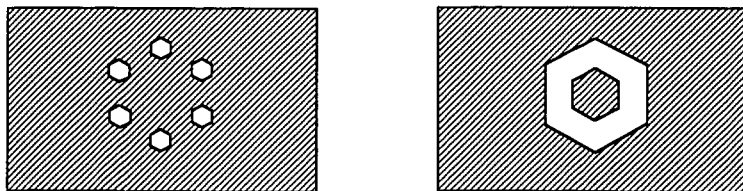


FIGURE 2. Development of pits in graphite from interaction with atomic hydrogen

Dispersed Catalysts for Coal Dissolution

Frank Derbyshire and Todd Hager

University of Kentucky Center for Applied Energy Research
3572 Iron Works Pike, Lexington, KY 40511-8433

Introduction

In 1988, one of the authors conducted a review of the status of catalysis in direct coal liquefaction.[1] The objectives were to assess the current state of knowledge and to identify new directions for research. The application of catalysts was addressed with respect to the two-stage processing concept, distinguishing the processes of primary coal dissolution and coal liquids upgrading.

Supported catalysts are quite adequate to the task of hydroprocessing distillate coal liquids. However, in the presence of high-boiling and non-distillable liquids, they are rapidly deactivated by the deposition of carbonaceous materials and metals. Furthermore, since large molecules cannot access the active catalyst surface, supported catalysts can only indirectly influence the processes of coal dissolution and residual coal liquids upgrading.

To surmount these problems, there are several possible approaches to developing new supported catalysts that are less prone to deactivation. However, it is also considered that there is considerable potential for improving liquefaction processing and economics through the development and appropriate application of highly dispersed catalysts. The principle objectives are to promote the process of primary coal dissolution and produce a solubilized product that can be upgraded with greater facility in a second stage over supported catalysts. Dispersed catalysts may also help to realize the potential of using cheap, low-rank coals as feedstocks by increasing the low rates and extent of conversion that are normally attained. Additionally, they may help to lower constraints on solvent quality, facilitating greater flexibility in the selection of recycle solvent fractions and the coprocessing of coals with petroleum residua.

This paper will address the use and development of coal dissolution catalysts. Emphasis will be given to iron-based catalysts because of cost considerations, and to their applicability to the liquefaction of low-rank coals.

Liquefaction of Low-Rank Coals

Before entering a discussion of dispersed catalysts, *per se*, some comments will be addressed to the liquefaction of low-rank coals. The present interest in these coals as liquefaction feedstocks relates to their lower cost, and to their ability to produce higher yields of low molecular weight products than bituminous coals.[2-4] It has been shown by comparative studies of processing bituminous and subbituminous coals that, in the latter case, the rate of deactivation of the second stage supported catalyst is lower and the resid is more reactive.[5] Against this, low-rank coals tend to convert more slowly and to lower ultimate conversions. Pilot plant experience has also shown that these coals can cause severe operating problems through the formation of deposits.[6]

The thermal liquefaction of low-rank coals proceeds with difficulty, due to their normally low content of catalytically active mineral matter and to the high reactivity of the organic structure. The latter allows crosslinking reactions to proceed at moderate temperatures, rendering the coal more difficult to dissolve. However, in the presence of a suitable catalyst, these phenomena can be suppressed and the potential for producing high distillate yields can be realized (Figure 1). [2]

Research by Keogh and Davis [7] has shown that the liquefaction pathways for bituminous coals and subbituminous coals are quite different. The triangular plot in Figure 2 shows the conversion routes followed by these coals from insoluble organic matter, to preasphaltenes and asphaltenes, to oil and gas. These data were developed from microautoclave experiments using a large number of coal samples, donor and nondonor solvents, and various supported and unsupported catalysts. What is found is that the two ranks of coal fall into different bands, and, as discussed above, oils are produced more directly from subbituminous coals, indicative of their being composed of smaller structural units. A second relevant finding is that, for a given coal, none of the variables affects the conversion pathway or conversion selectivity, and the only measurable effect is to increase the conversion kinetics. Thus it seems that selectivity can only be influenced by choice of feedstock, but that appropriate catalysts can improve the rate of conversion.

Dissolution Catalysts

The activity of dissolution catalysts is considered to depend on their composition and the extent of their dispersion and intimate contact with the coal-solvent slurry. These are interrelated factors, since the composition of the catalyst precursor will determine the methods that can be used for its addition and dispersion, and the efficacy of its conversion to an active form.

The extent of dispersion over, and in, the solid coal, and in the coal-solvent slurry, is directly related to the catalyst effectiveness. Until the coal is dissolved, there is no available mechanism by which reactants can be transported to the catalyst, and hence the basic requirement is to transport the catalyst to the reacting species. Overwhelming evidence has accumulated to demonstrate that catalyst activity is enhanced by introducing the precursor in a form more conducive to attaining high dispersion. [8]

There are no really satisfactory techniques for measuring high levels of dispersion. Its attainment and maintenance is inferred from the results of liquefaction experiments, and it is not usually possible to distinguish unequivocally the influence of other factors. For example, the rate of conversion of the precursor to a sufficiently active form may be too slow to influence the process of coal dissolution. The active form of catalysts such as Fe and Mo is generally believed to be a sulfide. In many cases, the attainment of this phase relies upon in-situ sulfiding, and there is scant information on the relative kinetics of dissolution and sulfiding reactions.

While direct comparisons are difficult, it is apparent that, all other things being equal, molybdenum is a much more active catalyst than iron. However, in the absence of suitable methods for catalyst recovery and/or recycle, the cost of Mo is considered prohibitive.

In the developments in Germany in the 1920s and 1930s, finely ground Mo catalysts were first used for the liquid phase hydrogenation of brown coal tar, initially at concentrations as high as 25%. [9] Effective results were subsequently obtained with much lower concentrations of Mo impregnated as ammonium molybdate solution onto brown coal char. Without the ability to separate and recover catalyst, attention was ultimately directed to using lower catalyst concentrations or lower cost catalysts. The impregnation of brown coal with ammonium molybdate allowed a concentration of 0.02% wt. of coal to be used. To reduce cost, iron ores were introduced at higher concentrations (2% wt of coal and higher). Iron compounds supplanted Mo on the brown coal char supports, and the effectiveness of the iron ores was later improved through their partial replacement by impregnating ferrous sulfate directly on the coal, which presumably aided dispersion.

For the same reasons, iron-based catalysts are preferred now, and there are considerable efforts to find means to enhance their activity. Much of this work is of a fundamental

nature and therefore it is not entirely reasonable to require economic justification. Nevertheless, it must be taken into account that the more exotic the preparation, the higher will be the cost, and that this could negate the basis for using iron as a starting point.

Directionally, the main approach to increasing catalytic activity is towards increasing the dispersion of the catalyst precursor and to maintaining this high dispersion after transformation to the active phase. Several techniques have been used to this end including the use of oil soluble organometallics, the synthesis of ultrafine particles, and the application of impregnation techniques to add the iron directly into the coal matrix.

High activities are reportedly favored by catalysts introduced as oil-soluble organometallic precursors such as naphthenates and carbonyls [10-15]. The work of Yamada et al. [13] showed that the catalytic effect of the cyclopentadienyliron dicarbonyl dimer $[(\text{FeCp}(\text{CO})_2)_2]$ is of the same order of magnitude as that of iron pentacarbonyl. The dicarbonyl dimer at a catalyst loading of 1 wt% Fe of resulted in an increase in conversion to THF solubles from 57% to 93% for an Illinois #6 bituminous coal at 425° C and 711 psig H_2 (cold) for 60 min. This compares favorably to the 92% conversion obtained for the same catalyst loading with the precursor molybdenum hexacarbonyl $(\text{Mo}(\text{CO})_6)$. The iron pentacarbonyl also showed the same high catalytic activity for a subbituminous Wandoan coal in the presence of added sulfur, resulting in a total conversion of 94%. Other iron carbonyls, $\text{Fe}_2(\text{CO})_9$ and $\text{Fe}_3(\text{CO})_{12}$, resulted in similar high conversions.[14] This indication that the iron carbonyls are effective catalyst precursors is supported by more recent experiments by Herrick et al. who used the iron pentacarbonyl precursor in coprocessing Illinois #6 bituminous coal with a Maya resid and found an increase in conversion to methylene chloride solubles from 39% to 82% at similar conditions to those used in the liquefaction studies but with an initial H_2 pressure of 1000 psig and a catalyst loading of 0.5 wt% Fe.

The addition of sulfur to the catalyst precursor can have a significant effect on the activity of some catalysts, particularly in the liquefaction of low sulfur coals. In the case of iron pentacarbonyl, the addition of elemental sulfur resulted in an increase of both the total conversion (~10%) and oils (~13%) for a low sulfur Wandoan coal.[13] For $\text{W}(\text{CO})_6$, the addition of sulfur increased the conversion from 52% to 94% and the oils from 14% to 57%. At a catalyst loading of 0.4 wt% Mo the total conversion for the precursor $\text{Mo}(\text{CO})_6$ increased by 17% while the oil yield increased by 13%. This indicates that while most of the organometallic precursors require sufficient sulfur for transformation to the active phase, the activity of iron is improved less by added sulfur than molybdenum or tungsten based precursors.

The results of some studies indicate that, even with soluble precursors, quite large crystallites or agglomerates can be formed during liquefaction and hence the potentially high dispersion is not realized or maintained. There is some evidence to indicate that, if the precursor is introduced as particulates, there is less tendency for agglomeration. Fine iron particles (50 nm mean diameter) synthesized by a flame pyrolysis technique appeared to have retained their particle size and shape during presulfiding and coal liquefaction.[16,17]

In this same context, efforts have been directed towards improving the dispersion of iron based catalyst precursors through the synthesis of ultrafine particles (UFPs) with diameters that can be significantly less than 100 nm. The increase in catalytic activity that is expected with decreasing particle size may be due to a combination of effects: an increase in exterior surface and an associated enhancement of sulfiding kinetics; a radical departure from bulk properties, especially with regard to surface energetics as the particle size is reduced below about 10 nm. The synthesis of ultrafine catalyst particles could therefore provide a means

to enhance the activity of dispersed iron (or other metal) catalysts. Several techniques have been used to produce this type of precursor, including pyrolysis in a flame or by laser.

The laser pyrolysis technique has been used to produce iron carbide UFPs from a mixture of iron pentacarbonyl and ethylene.[18] Particles of Fe_3C and Fe_7C_3 have been produced with average particle diameters of 4-20 nm. In this research, the synthesis of carbides was primarily intended as a starting point from which to establish procedures for the synthesis of oxide, sulfide, and mixed-metal phases. Although it is generally considered that the active phase of Fe and Mo is a sulfide form, recent studies by Oyama and co-workers have shown that supported and unsupported Mo carbides and nitrides exhibit high activity for hydrodenitrogenation and hydrodesulfurization reactions [19-21], raising the possibility that the carbides and nitrides of Mo and other metals may be active liquefaction catalysts.

Liquefaction studies were conducted with the Fe_3C and Fe_7C_3 UFPs using a subbituminous Wyodak coal at 385 °C, 800 psig H_2 (cold) for 15 minutes in the presence of sulfur added as dimethyldisulfide. The results of these experiments demonstrated that, under these conditions, the particles exert only a moderate catalytic effect that is slightly less than that of the oil soluble precursor iron naphthenate. At 400°C the particles increase the total conversion by ~10% above the thermal baseline. Mössbauer studies of the liquefaction residues show that, unlike the Mo carbides mentioned above, the particles are sulfided and transformed to pyrrhotite. The different response of Fe and Mo carbides to sulfiding may well relate to the much higher stability of the latter.

The moderate performance of the iron carbide UFPs may be attributable to a number of causes relating to the unusual properties of nanometer size particles, and may not be an accurate reflection of their intrinsic activity. The particles, as synthesized, are pyrophoric and the present procedure involves slow stabilization in an O_2/He mixture to allow handling in air. The method produces a surface oxide coating. Trapping the particles directly in a solvent or coal-solvent slurry may obviate this problem. The particles also tend to agglomerate, possibly aided by magnetic effects, and techniques must be developed to ensure their efficient dispersion. Thermal stability is another factor: in-situ X-ray diffraction studies have shown that sintering starts in the region of 300°C; experiments conducted under liquefaction conditions, and in the absence of coal, show that the particles are very susceptible to sintering but, in the presence of added sulfur, this tendency is reduced. Neither are there, as yet, data on the comparative kinetics of sulfiding and coal dissolution, and the prospect exists catalyst may not be present in an active form while critical reactions are taking place in the coal.

A second example of UFP synthesis is the formation of aerosol oxides formed by the combustion of metal chlorides in a hydrogen-oxygen flame.[22,23] These particles have diameters around 50 nm and surface areas between 20 and 50 m^2/g . The iron oxide aerosols have demonstrated a high catalytic activity in the presence of added sulfur at a catalyst loading of 2% for the liquefaction of a bituminous coal at 350 °C and 2000 psig H_2 (cold) for 60 minutes. The results show a doubling of the total conversion from 25% to 52%. This was only slightly less than that produced by a molybdenum aerosol generated by the same technique. This catalytic effect is reduced at higher temperatures. Again, as with the other iron based catalysts, XRD of the liquefaction residues indicate the transformation of the Fe_2O_3 aerosol to pyrrhotite in the presence of sulfur.

The use of an incipient wetness technique to impregnate the coal with Fe^{3+} from an aqueous solution has been shown to give high dispersion of the catalyst precursor on a coal substrate [24]. The coal matrix also aids in maintaining the high dispersion subsequent to activation. At a catalyst loading of 2500 ppm the precipitated FeOOH yielded the same

catalytic activity as 1500 ppm molybdenum, added as ammonium heptamolybdate, for the liquefaction of an Illinois #6 coal at 425 °C and 2500 psig H₂ for 1 hour. The addition of sulfur was necessary to cause the transformation to the active form. The transition of amorphous iron to crystalline pyrrhotite occurred between 300° C and 350° C, although pyrrhotite is probably present below 350° C in particles with diameters less than 10 nm.

The application of Mössbauer and EXAFS spectroscopies to the study of iron based catalysts has been very informative. Studies conducted by Huffman et al. [25] used a variety of catalyst precursors including Fe₂O₃ on carbon black, Fe₂O₃/SO₄²⁻, iron added by cation exchange, and chemical impregnation by FeCl₃. The primary form of the as-dispersed iron catalyst was shown to be either an oxide or oxyhydroxide. The introduction of catalyst by ion exchange techniques showed that the iron formed small crystallites of superparamagnetic FeOOH.

Modified Iron Catalysts

Another route to improving the activity of iron catalysts is to modify their composition. One approach has been to change the surface properties of hematite particles by treating a precipitated FeOOH with H₂SO₄. [26,30] Studies of these particles after calcining indicate the formation of Fe₂O₃/SO₄²⁻. This notation denotes SO₃ chemisorbed on the surface of Fe₂O₃ in a nonstoichiometric relation. The sulfate group is believed to be responsible for the superacidity displayed by these particles. The addition of the sulfate group also leads to a decrease in the average crystallite size, which is believed to be the primary reason for their enhanced activity. Liquefaction studies using an Illinois #6 coal at 400 °C and 1000 psig H₂ (cold) for 1 hour showed an increase in the total conversion from 65 % to 90 %, in the presence of added sulfur, for a catalyst loading of 0.35 wt. %. Similar enhanced activity was seen for the liquefaction of a subbituminous Wyodak coal. Analysis of the liquefaction residues indicate that the majority of the catalyst had been transformed to pyrrhotite with only traces of oxide phases remaining.

There are a number of instances in the literature which show that metals in combination can be more effective catalysts than they are individually. The presence of titanium in the German "red mud" catalyst has been suggested to promote the activity of iron. Other research has shown that titanium can promote the activity of molybdenum, leading to significant increases in distillate production, as shown in Figure 3. [27]

It has been found that the effectiveness of an iron catalyst can be greatly improved by the addition of small concentrations of molybdenum, such that the combination has the same activity or higher than much higher concentrations of Mo alone. [28,29] The addition of 20 - 100 ppm Mo to the Fe₂O₃/SO₄²⁻ was found to increase the oil yields as well as the total conversion in the coprocessing of an Illinois # 6 coal. [30] The incorporation of 2% Mo to the iron oxide aerosol particles formed by flame pyrolysis showed a significant increase in conversion for both a bituminous and a subbituminous coal. [31] The activity of the Mo doped aerosol particles was higher than that of a supported Ni-Mo catalysts despite the higher concentration of Mo present in the supported catalyst.

These studies have shown that by the addition of low concentrations of promoter metals, the activity of iron catalysts can be enhanced either to provide increased performance at the same concentration or equivalent performance at reduced concentrations. In either case, gains could be made at marginal extra catalyst cost which retains the "disposability" of the catalyst while effecting process economies which more than compensate.

Intermetallic hydrides have also been the subject of investigations. These alloys form reversible metal hydrides that can store molecular hydrogen within the metal matrix at

densities greater than that of liquid hydrogen. Several of these alloys have shown some activity as liquefaction catalysts.[32,33] In studies using a hvA bituminous coal, the activity of these intermetallic hydrides was shown to follow the trend $\text{CaNi}_5 = \text{LaNi}_5 > \text{FeTi} > \text{Mg}_2\text{Cu} > \text{Mg}_2\text{Ni}$, although the variation between the higher three is less than 5%. The highest activity resulted in a doubling of the total conversion over a noncatalytic baseline at temperatures between 370 °C and 427 °C. There has also been speculation that the enhanced activity of iron aerosols in the presence of added tin aerosols is due to the transitory formation of an intermetallic hydride that is unstable at room temperature.[34]

References

- 1) Derbyshire, F. J., IEACR/08, London, UK, IEA Coal Research, 69 pp (1988)
- 2) Wu W R K, Storch H H, 1968, Hydrogenation of Coal and Tar. Bulletin 633, Washington, DC, USA, US Department of the Interior, Bureau of Mines, 195pp.
- 3) Derbyshire F J, Stansberry P G, 1987, *Fuel*, **66**, 1741-2
- 4) Tomlinson G C, Gray D, Neuworth M B, Talib A, Report SAND85-7238, Albuquerque, NM, USA, Sandia National Laboratories, 105pp.
- 5) El Sawy A, Gray D, Talib A, Tomlinson G, 1986, Report SAND86-7103, Albuquerque, NM, USA, Sandia National Laboratories, 198pp.
- 6) Nakako, Y.; Ohzawa, T.; Narita, H., 1991 ICCS Proceedings, Oxford, UK, Butterworth-Heinemann, 652-5 (1991).
- 7) Keogh, R. A.; Davis, B. H., *ACS Div. of Fuel Chem. Preprints*, **36**(2) 438-44 (1991).
- 8) Weller, S.; Pelipetz, M. G., *I&EC Eng. & Proc. Dev.* **43**(5) 1243-6 (1951).
- 9) Donath, E. E.; Hoering, M., *Fuel Proc. Tech.*, **1** 3-20 (1977).
- 10) Watanabe, Y.; Yamada, O.; Fujita, K.; Takegami, Y.; Suzuki, T., *Fuel*, **63** 752-5 (1984).
- 11) Suzuki, T.; Yamada, O.; Then, J. H.; Ando, T.; Wantanabe, Y., Proceedings- 1985 ICCS, Sydney, NSW, Australia, Pergamon Press, 205-8 (1985).
- 12) Hirschon, A. S.; Wilson, R. B., "Designed Coal Liquefaction Catalysts", *ACS Div. of Fuel Chem. Preprints*, **36**(1) 103-7 (1991).
- 13) Yamada, O.; Suzuki, T.; Then, J. H.; Ando, T.; Wantanabe, Y., *Fuel Proc. Tech.*, **11** 297-311 (1985).
- 14) Suzuki, T.; Yamada, O.; Takahashi, Y.; Wantanabe, Y., *Fuel Proc. Tech.*, **10** 33-43 (1985).
- 15) Herrick, D. E.; Tierney, J. W.; Wender, I.; Huffman, G. P.; Huggins, F. E., *Energy and Fuels*, **4**(3) 231-6 (1990).
- 16) Andres, M.; Charcosset, H.; Chiche, P.; Djega-Mariadassou, G.; Joly, J-P.; Pregermain, S., Preparation of Catalysts III (eds. G. Poncelet and P. Grange), Elsevier, 675-82 (1983).
- 17) Andres, M.; Charcosset, H.; Chiche, P.; Davignon, L.; Djega-Mariadassou, G.; Joly, J-P.; Pregermain, S., *Fuel* **62** 69-72 (1983).
- 18) Hager, G. T.; Bi, X. X.; Derbyshire, F. J.; Eklund, P. C.; Stencel, J. M., *ACS Div. of Fuel Chem. Preprints*, **36** (4) 1900-8 (1991).
- 19) Oyama, S. T.; Schlatter, J. C.; Metcalfe, J. E.; Lambert, J. M., *I&EC Research*, **27**, 1639-48 (1988).
- 20) Schlatter, J. C.; Oyama, S. T.; Metcalfe, J. E.; Lambert, J. M., *I&EC Research*, **27**, 1648-53 (1988).
- 21) Sajkowski, D. J.; Oyama, S. T., *ACS Div. of Fuel Chem. Preprints*, **35** (2) 233-36 (1990).
- 22) Bacaud, R., *Applied Catalysis*, **75** 105-17 (1991).
- 23) Cebolla, V. L.; Diack, M.; Oberson, M.; Bacaud, R.; Cagniant, D.; Nickel-Pepin-Donat, B., *Fuel Proc. Tech.*, **28**(2) 183-201 (1991).

- 24) Cugini, A. V.; Utz, B. R.; Krastman, D.; Hickey, R. F.; Balsone, V., ACS Div. of Fuel Chem. Preprints, **36** (1) 91-102 (1991).
- 25) Huffman, G. P.; Ganguly, B.; Taghiei, M.; Huggins, F. E.; Shah, N., ACS Div. of Fuel Chem. Preprints, **36**(2) 561-9 (1991).
- 26) Pradhan, V. R.; Tierney, J. W.; Wender, I.; Huffman, G. P., "Catalysis in Direct Coal Liquefaction by Sulfated Metal Oxides", *Energy & Fuels*, **5** 497-507 (1991).
- 27) Wilson, T. P.; Hurley, G. F., Technical Report 84002-1-4950, Union Carbide Olefins Company, South Charleston, WV, USA, 125pp, (1960)
- 28) Derbyshire, F. J.; Davis, A.; Schobert, H. H.; Stansberry, P. G., ACS Div. of Fuel Chem. Preprints, **35**(1) 51-60 (1990).
- 29) Garg, D.; Givens, E. N., ACS Div. of Fuel Chem. Preprints, **28**(5) 200-9 (1983).
- 30) Pradhan, V. R.; Herrick, D. E.; Tierney, J. W.; Wender, I., *Energy & Fuels*, **5**(5) 712-20 (1991).
- 31) Bacaud, R.; Charcosset, H.; Jamond, M., *Fuel Proc. Tech.*, **24** 163-9 (1990).
- 32) Johnson, S. D.; Smith, J. E. Jr., *Applied Catalysis*, **44**(1-2) 53-71 (1988).
- 33) Smith, J. E. Jr.; Johnson, S. D., ACS Div. of Fuel Chem. Preprints, **35**(1) 823-30 (1990).
- 34) Besson, M.; Bacaud, R.; Brodski, D.; Bussiere, P.; Charcosset, H.; Djega-Mariadassou, G.; Oberson, M.; Sharma, B. K., *Fuel*, **69** 35-43 (1990).

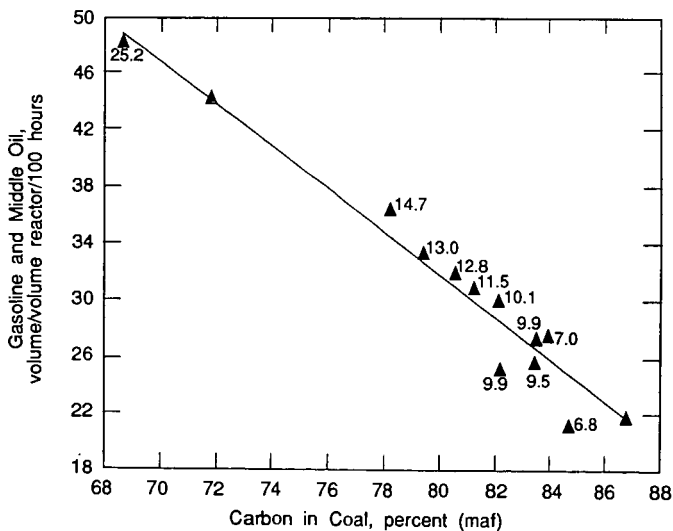


Figure 1. Yield of Gasoline Plus Middle Oil in Relation to Coal Rank
(Numbers Indicate Oxygen Content)

(Adapted from Wu and Storch, [2])

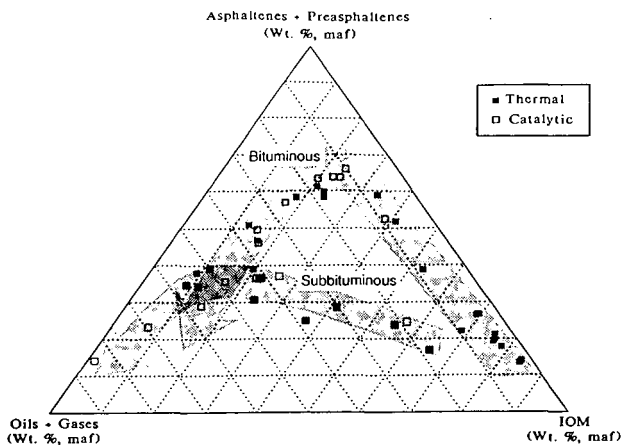


Figure 2. Liquefaction Pathways for Bituminous and Subbituminous Coals. (from Keogh and Davis[7])

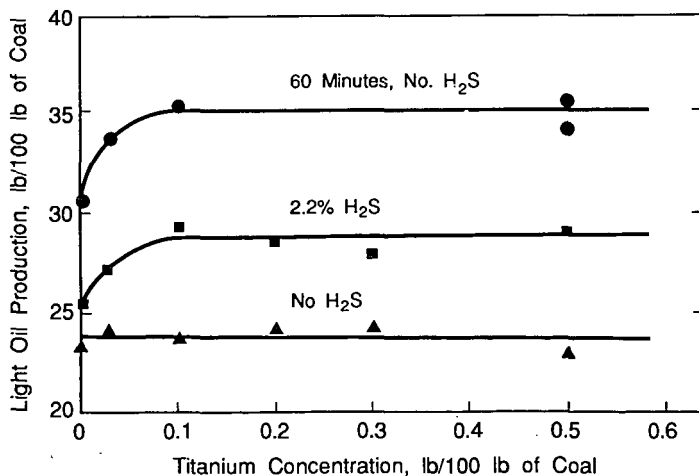


Figure 3. The Promotional Effect of Titanium on Molybdenum for Light Oil Production (0.2% Molybdenum; 480°C; 4400 psi H₂)

(From Wilson and Hurley [27])

ADVANCES IN THE MODELLING OF LIGAND-ACCELERATED HETEROGENEOUS REACTIONS

M. Garland^a, H.P. Jalett,^b H.U. Blaser^b

(a) Department of Chemical Engineering,
Swiss Federal Institute of Technology,
Universitatstrasse 6, CH-8092 Zurich,
Switzerland (b) Central Research Services,
CIBA-GEIGY AG, R1055.6, CH-4002
Basel, Switzerland

INTRODUCTION

The term ligand-accelerated catalysis first appeared in conjunction with the osmium catalyzed dihydroxylation of alkenes.¹ In this reaction, a chiral auxiliary, normally a natural occurring cinchona alkaloid, is added to a solution containing OsO₄ and alkene. The resulting homogeneous system, leads to both the enantiomeric excess of one diol as well as a marked increase in reaction rate.

In addition to a dramatic 1-2 orders of magnitude increase in reaction rate, a remarkable interdependence between the optical yield (ee) and rate at low concentrations of chiral modifier is observed.² This interdependence can be easily recognized by examining simultaneous plots of ee and rate versus modifier concentration. Such plots exhibited a strong increase in rate, but an even more spectacular increase in ee, as a function of modifier. Indeed, such characteristic plots give the impression that a maximum ee is reached long before the maximum rate for the system is attained.

The heterogeneous and enantioselective hydrogenation of α -keto esters, catalyzed by cinchona modified Pt/Al₂O₃ was first reported by Orito et al.^{3,4} Initial studies with both the unmodified (racemic) and

fully modified (enantioselective) Pt/Al₂O₃ systems showed that the rate of hydrogenation for the latter was roughly 1 order of magnitude higher.⁵ Indeed, at 20°C and 10.0 MPa hydrogen the measured turnover frequency for the fully modified system approaches 50 s⁻¹.⁶ However, mass transfer control can be avoided by using a powdered catalyst, low loadings and a proper level of agitation.⁶

Subsequent studies were carried out with trace quantities of cinchona (modifier/Pt_T \leq 1).⁷ These experiments confirmed that both ee and rate were continuous functions of the cinchona concentration. Moreover, these functions yielded the characteristic types of curves indicative of a ligand accelerated reaction. With a modifier to Pt_T concentration as low as 0.25 in toluene,⁷ or less than 0.10 in acetic acid,⁸ maximum optical yields can be obtained.

The interdependence of ee and rate for the cinchona modified Pt/Al₂O₃ systems, were successfully analyzed in the context of a two-cycle mechanistic scheme. After imposing a mass balance constraint on the total platinum in the system, a simple relationship between ee and rate arises (Eq 1). This slope-intercept form correctly describes the interdependence of ee and rate for experiments conducted in toluene and ethanol as solvents.⁷

$$ee_{obs} = a + b/r_{obs} \quad 1$$

$$a = 100(2s-1)k_m/(k_m - k_u)$$

$$b = 100(2s-1)k_u k_m Pt_T / (k_m - k_u)$$

In the following, Eq 1 is modified to include a stoichiometry for the modified platinum sites. The data from toluene experiments are then re-examined. Emphasis is given to (i) the turnover frequency based on the number of modified sites and (ii) the form of the adsorption isotherm.

EXPERIMENTAL

The 5% Pt/Al₂O₃ catalyst used in this study (Engelhard 4759) had a mean particle size of 55 μm, a BET surface area of 140 m²/g, a mean pore radius of 50 Å, a real density of 5.0 g/ml, and a dispersion of 0.28.⁶

A 50 ml batch reactor, with cooling jacket, baffles, a 3 cm magnetic stirring bar, a thermocouple, and a capillary sampling line, was used for all kinetic experiments. A 45 ml reservoir, pressure regulators, pressure transducers and a cryostat were connected to the reactor. The reactor could be maintained isothermal ΔT = 0.3°C, and isobaric ΔP = 0.1 MPa for the duration of an experiment.

Typically, 100 mg catalyst (pretreated 2 hours in H₂ at 400°C), 0.2 mg 10,11-dihydrocinchonidine (HCD), 10 ml ethyl pyruvate and 20 ml solvent were charged to the reactor. The system was then purged 5 times with argon under stirring.

In the absence of stirring, the reservoir and reactor were pressurized with hydrogen. After 2-3 minutes, both the stirrer and data acquisition were started. Initial rate data was analyzed after the 30 second saturation period. Optical yields were determined after derivatization followed by glc.⁶

RESULTS AND DISCUSSION

Basic Derivation for EE and Rate First, consider a mass balance for the total platinum surface atoms Pt_T in an experiment, in terms of unmodified and modified platinum atoms and also the degree of surface modification x_m.

$$Pt_T = Pt_u + Pt_m \quad 2$$

$$x_m = Pt_m/Pt_T \quad 3$$

The observed rate of product formation can then be written (i) in terms of the modified and unmodified rates (ii) by including pseudo first order rate constants k_u and k_m (iii) by including the variable x_m.

$$r_{obs} = r_u + r_m \quad 4$$

$$r_{obs} = k_u Pt_u + k_m Pt_m \quad 5$$

$$r_{obs} = [(1-x_m)k_u + x_mk_m]Pt_T \quad 6$$

By introducing an intrinsic selectivity s for the modified sites, expressions can be written for the rate of formation of the R and S enantiomers as well.

$$r_R = 0.5k_u Pt_u + sk_mk_m Pt_m \quad 7$$

$$r_S = 0.5k_u Pt_u + (1-s)k_mk_m Pt_m \quad 8$$

Using only the variables defined above, and the definition of ee, two new expressions can be written for the observed optical yields ee_{obs}.

$$ee_{obs} = 100(r_R - r_S)/(r_R + r_S) \quad 9$$

$$ee_{obs} = 100(r_R - r_S)/r_{obs} \quad 10$$

$$ee_{obs} = [100(2s-1)x_mk_m Pt]/r_{obs} \quad 11$$

Further, rearranging Eq 6 gives:

$$x_m = [(r_{obs}/Pt_T) - k_u]/(k_m - k_u) \quad 12$$

Finally, elimination of x_m from Eq 11 leads to the interdependence between ee and rate (or TOF).

$$ee_{obs} = a + b/TOF \quad 13$$

$$a = 100(2s-1)k_m/(k_m - k_u)$$

$$b = 100(2s-1)k_u k_m/(k_m - k_u)$$

Comment I. For data which conforms to the slope-intercept form of Eq 13, the condition m < 0 represents a ligand

accelerated reaction, whereas the condition $m > 0$ represents a ligand decelerated reaction.

The numerical value of k_u can always be obtained from an unmodified experiment or from the relationship $k_u = b/a$. Further, if the system is entirely modifiable, or if one explicitly assumes $(x_m)_{\max} = 1$, then it is possible to solve for k_m and s . Otherwise k_m and s remain undetermined.

Comment II. The above derivation avoids a number of potential problems. Foremost, the exact relationship between the quantity of modifier and the number of modified platinum sites is unknown, and may well differ from system to system. For example, we don't know if the system obeys a simple Langmuir adsorption isotherm, and there may well be some adsorption on the support. (See Comment IV)

The final expression for a two-cycle system Eq 13, involving just e and rate, and free from both $[HCd]$ and x_m , was tested on the toluene system.⁷ A very good linear correlation was obtained, namely, $s = 0.93 \pm 0.02$, $k_u = 1.03 \pm 0.07 \text{ s}^{-1}$ and $k_m = 10.0 \pm 0.7 \text{ s}^{-1}$.

Inclusion of Stoichiometries. Clearly, it is an oversimplification to assume that each platinum atom is a site. This is particularly true for modified sites Pt_m , where adsorption of modifier ($MW \approx 300$) certainly requires an ensemble of platinum atoms. Accordingly, we define a modified site Pt^* in terms of a stoichiometry ν_m of modified atoms. Additionally, a new consistent rate constant k^* for a modified site can be defined.

$$Pt^* = Pt_m / \nu_m \quad 14$$

$$k^* = \nu_m k_m \quad 15$$

$$r_m = k^* Pt^* \quad 16$$

Next, let us assume that a modified site consists of a single cinchona molecule and an ensemble of platinum atoms. The quantity of adsorbed modifier $[HCd]_{ad}$ can be defined in terms of the number of modified sites, and in terms of an appropriate equilibrium constant.

$$[HCd]_{ad} = Pt^* \quad 17$$

$$[HCd]_{ad} = K_{eq} [HCd]_{soln} Pt_u \quad 18$$

Finally, there is the implicit assumption that all platinum atoms are modifiable. This is almost certainly not the general case. As a very simple example, consider platinum crystallites in very narrow pores ($< 10 \text{ \AA}$). Such atoms are almost certainly inaccessible to the modifier.

Accordingly, the total number of surface platinum atoms which are potentially modifiable, is considerably less than the number of surface platinum atoms i.e. $Pt_T \leq Pt_{surf}$, and we can write:

$$Pt_T = \xi Pt_{surf} \quad 19$$

$$0 \leq \xi \leq 1 \quad 20$$

Comment III. If the adsorption of a cinchona molecule is very strong, i.e. the equilibrium constant is very large, then the number of modified platinum atoms and the fraction modification are simply:

$$Pt_m = \nu_m [HCd]_T \quad 21$$

$$x_m = \nu_m [HCd]_T / Pt_T \quad 22$$

At this point, the rate of reaction can be rearranged, and its derivative with respect to $[HCd]_T$ can be taken. This provides a very good estimate of the magnitude of the pseudo first order rate constant k^* for a modified site when the condition $k_u \ll k_m$ is fulfilled.

$$r_{obs} = [k_u + x_m(k_m - k_u)] Pt_T \quad 23$$

$$r_{\text{obs}} = (k_v/Pt_T) + v_m[\text{HCd}]_T(k_m - k_u)$$

$$dr_{\text{obs}}/d[\text{HCd}]_T = v_m(k_m - k_u) \quad 25$$

$$dr_{\text{obs}}/d[\text{HCd}]_T \approx k^* \quad 26$$

The minimum value of the rate constant k^* for experiments conducted in toluene as solvent at 20°C is $k^* \approx 130 \text{ s}^{-1}$. If the above assumptions concerning strong adsorption and stoichiometry are correct, then k^* is the effective turnover frequency per molecule of dihydrocinchonidine!

Comment IV. The product of ee and TOF is a very interesting function because it serves as a measure for the fraction modification x_m . Such a measure can suggest an appropriate form for an adsorption isotherm between dihydrocinchonidine molecules and the platinum surface.

$$ee \cdot \text{TOF} = 100(2s-1)k_m x_m \quad 27$$

A plot of (ee•TOF) versus $[\text{HCd}]_T/Pt_{\text{surf}}$ is shown in Figure 1. Clearly, the results for the cinchona and $\text{Pt}/\text{Al}_2\text{O}_3$ system are in agreement with a simple Langmuir adsorption isotherm, with no further complication or qualifications.

The above result is interesting because it has been suggested that enantioselection in the cinchona system arises due to a *well ordered array* of adsorbed modifier.^{9,10} The results presented in Figure 1 strongly argue against such a suggestion. Indeed, the formation of a well ordered array or even the statistically random aggregation of 3 or 4 modifier molecules, as the source of enantioselection, would not lead to the simple, continuous and asymptotically increasing form shown in Figure 1.

This latter result strongly suggests that an enantioselective site consists of *one cinchona alkaloid molecule and an ensemble of platinum atoms*.

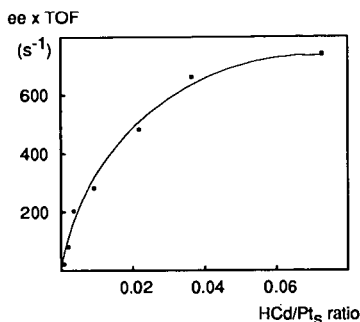


Figure 1. The function (ee•TOF) versus $[\text{HCd}]_T/Pt_{\text{surf}}$ for data taken in ethanol as solvent. (See Eq 27)

A considerably more complex relationship exists between ee and rate at yet higher loadings of chiral modifier in both toluene and ethanol as solvent and at high loadings in acetic acid.

REFERENCES

- [1] Jacobsen, E.N.; Marko, I.; Mungall, W.S.; Schröder, G.; Sharpless, K.B. *J. Am. Chem. Soc.* **1988**, *110*, 1968.
- [2] Jacobsen, E.N.; Marko, I.; France, M.B.; Svendsen, J.S.; Sharpless, K.B. *J. Am. Chem. Soc.* **1989**, *111*, 737.
- [3] Orito, Y.; Imai, S.; Niwa, S. *J. Chem. Soc. Jpn.* **1979**, 1118.
- [4] Orito, Y.; Imai, S.; Niwa, S. *J. Chem. Soc. Jpn.* **1980**, 670.
- [5] Blaser, H.U.; Jalett, H.P.; Monti, D.M.; Reber, J.F.; Wehrli, J.T. *Stud. Surf. Sci. Catal.* **1988**, *41*, 153.
- [6] Garland, M.; Blaser, H.U. *J. Am. Chem. Soc.* **1990**, *112*, 7048.
- [7] Garland, M.; Jalett, H.P.; Blaser, H.U. *Stud. Surf. Sci. Catal.* **1991**, *58*, 177.
- [8] Blaser, H.U.; Jalett, H.P.; Wiehl, J.J. *Mol. Cat.* **1991**, *68*, 215.
- [9] Thomas, J. *Angew. Chem. Adv. Mater.* **1989**, *101*, 1105.
- [10] Wells, P.B. *Faraday Discuss. Chem. Soc.* **1989**, *87*, 1.

Fuel Chemistry Division Invited Paper
Spring ACS Meeting April 5-10, 1992, San Francisco, CA
last revision: January 9, 1992

COMPUTATIONAL APPROACH TO THE PREDICTION OF BIMETALLIC CLUSTERS

PREPRINTS OF THE FUEL CHEMISTRY DIVISION, ACS

Liqiu Yang, Todd J. Raeker, Ann M. Schoeb, Xi Wu,
Terry King and Andrew E. DePristo
Ames Laboratory, USDOE
Iowa State University, Ames, IA 50011

Keywords

structure of bimetallics; corrected effective medium theory; partial bond energies

Abstract

The catalytic properties of bimetallic clusters will be influenced by the detailed structure of the cluster surface. Enrichment of one metal at the surface is one feature of obvious importance. Other, less obvious, features are preferential population of edge and corner binding sites on the surface and micromixing that influences ensemble size on the surface planes.

We review the range of methods developed to treat this problem, from the computationally demanding corrected effective medium (CEM) theory (a semi-empirical density functional based method) to the computationally simple method of partial bond energies. Parametrization of the latter is shown to be feasible using the former.

Comparisons of theoretical predictions with experimental data will be made for heats of formation in selected alloys and for surface segregation behavior in $\text{Rh}_{0.9}\text{Pt}_{0.1}(111)$. Detailed results on the shape, site composition and surface micromixing will be shown for selected systems chosen from $\text{Rh}_x\text{Pd}_{1-x}$, $\text{Ni}_x\text{Pd}_{1-x}$, and $\text{Rh}_x\text{Ni}_{1-x}$, $\text{Rh}_x\text{Pt}_{1-x}$ and $\text{Pt}_x\text{Cu}_{1-x}$ with $x=[0,1]$ for sizes between 200 and 1200 total atoms.

Introduction

The prediction of structure and energies of bimetallic clusters in the range of 200-2000 atoms provides an important technological problem for fundamental descriptions of metal-metal bonding. These systems are relevant to the performance of bimetallic catalysts¹ and also small enough to be treated by reasonably accurate theoretical density functional theory methods.²⁻⁴ They are also large enough to be treatable by empirical bonding models.⁵⁻⁷ Thus, such systems can provide an excellent testing ground for theoretical methods as well as demonstrate the utility of new theoretical methods in conjunction with rapidly advancing computer technology.

Theory

A hierarchy of theories have been used to describe bimetallics. We give a brief overview of each here. The reader interested in more details should consult the references, especially ref.(2d) for CEM, ref.(2c) for MD/MC-CEM and ref.(4) for construction of embedding functions in either theory. Applications to bimetallic

surfaces can be found in ref.(3). For the method of partial bond energies, the reader should consult refs.(5-7) for an overview.

For a set of N-atoms, $\{A_i, i=1, \dots, N\}$, the CEM theory utilizes the following equations to calculate the interaction energy:

$$\Delta E(\{A_i\}) = \sum_{i=1}^N \Delta E_{LMTO}(A_i; n_i) + \frac{1}{2} \sum_{i=1}^N \sum_{j=1}^N V_c(i, j) + \Delta G(\{A_i\}) \quad (1)$$

$$n_i = \frac{1}{2Z_i} \sum_{j=1}^N \int n(\vec{r} - \vec{R}_i) n(\vec{r} - \vec{R}_j) d\vec{r} \quad (2)$$

$n(\vec{r} - \vec{R}_i)$ is the unpolarized atomic electron density distribution (from Hartree-Fock calculations) while Z_i and \vec{R}_i are the atomic number and nuclear position, respectively. This equation is valid under the assumption that the total system electron density can be approximated as the superposition of atomic electron densities.

The first term is the sum of the embedding energy for each atom, *each term of which is solely a function of the average electron density environment of that particular type of atom*. The subscript 'LMTO' indicates that these are provided by forcing the CEM method to duplicate the results of self-consistent Linearized Muffin Tin Orbital density functional calculations on the cohesive energy of the homogeneous bulk solid at lattice constants from 30% expansion to 10% contraction.^{4a} Since these embedding energies are a major component of the system interaction energy, it is important to determine them accurately and this procedure does so, at least for coordinations approaching that of the bulk. For very low coordinations, it is necessary to supplement the LMTO calculated values with experimental data from the diatomic binding curve.^{4b}

The second term consists of pairwise additive coulombic energies. $V_c(i, j)$ is the sum of electron-electron, electron-nuclear and nuclear-nuclear coulomb interactions between atoms A_i and A_j . These are determined from the electron densities of each atom and are not adjustable.

The last term, ΔG , is the difference in kinetic-exchange-correlation energies of the N-atom and atom-in-jellium systems. It is a true many body term which is extremely time consuming computationally since it involves computation of a three dimensional multicenter integral of complicated functions of both the electron density and its gradient with respect to electronic coordinates.

To lower the computational effort, a simpler theory has been developed with acronym MD/MC-CEM since it is fast enough to use in direct MD and MC simulations of large systems. In this method, the ΔG term is approximated as a function of n_i and incorporated into new effective embedding terms. This yields the working equation as:

$$\Delta E(\{A_i\}) = \sum_{i=1}^N \Delta F_{LMTO}(A_i; n_i) + \frac{1}{2} \sum_{i=1}^N \sum_{j=1}^N V_c(i, j) \quad (3)$$

The effective embedding functions, ΔF_{LMTO} are determined again from LMTO calculations on the homogeneous bulk system.

The above two methods involve continuous change in interaction energies with separations between atoms. Neither is pairwise additive, and thus describes the delocalized bonding in metals. The CEM method can be derived from the fundamental density functional theory under the assumption of additive atomic densities. The MD/MC-CEM method is more empirical, depending upon a rather uncontrolled approximation to the kinetic-exchange-correlation energy difference energy. This method is very similar to the EAM method which simply postulates a form like Eq.(3) and replaces all terms by empirical forms. (e.g. Morse potentials or shielded coulomb like terms for the two body interactions).^{8,9} The EAM approach also utilizes the density at the nucleus of atom A_i instead of the average in Eq.(2), to identify a jellium density.

We have also utilized a much simpler formulation than either CEM theory. This calculates the energy of an atom by counting the bond energies with each of its nearest neighbors, adjusting the strength of each bond according to the number of neighbors. This is the method of partial bond energies and leads to the working equation for a system of one atom type:

$$\Delta E ([A_i]) = \sum N_i \epsilon (A_i ; N_i) \quad (4)$$

where $\epsilon(A_i;N_i)$ is the bond energy of atom A_i with N_i nearest neighbors. This equation must be supplemented with the interchange energy when there are different types of atoms.⁵ Note that bond lengths are not required in the application of this method because the interatomic potential is a function of coordination rather than distance. However, this approach does require the assumption that the metal particle maintains a fixed lattice type during the simulation. In the results reported below the simulations are fixed in an fcc lattice.

The connection between these methods is that the CEM theory can be used to provide the partial bond energies by using selected calculations on various metal surfaces and metal vacancy formation.¹⁰

Results and Discussion

First, consider the Rh_xPt_{1-x} system. The surface energies (in J/m^2) predicted by CEM (MD/MC-CEM) are 2.37 (2.73), 2.52(2.88) and 2.71 (3.12) for Rh(111), Rh(100), Rh(110), respectively.^{4a} Experimental data on surface free energies of polycrystalline samples¹¹ at the metal's melting point and at 298 K can be used to extrapolate to 0 K with the result being 2.94 J/m^2 . The agreement is excellent as it is for other fcc metals.^{4a} The CEM predictions of the alloy formation energy are -2.4, -2.2 and -1.7 kJ/mole for $x=0.75$, 0.5 and 0.25 respectively. Since Pt and Rh alloy even at low temperatures, this small negative alloy formation energy is very reasonable. The MD/MC-CEM method predicts 42.0, 53.3 and 39.1 kJ/mole, respectively, and is thus inaccurate for this system. Indeed, we have found that MD/MC-CEM is inaccurate for all mixtures of Ir, Pt and Au with all other metals, except Ir,Pt and Au.

Using CEM calculations of the various Pt and Rh systems yields the partial bond energies shown in Fig.(1). For comparison, partial bond energies using a quadratic fit to limited experimental data are also shown. The agreement is quite good except at very low coordinations where the previous approach involves extrapolation.

Predictions of the surface fraction of Rh in Rh_xPt_{1-x} bimetallics cluster with 201 total atoms is shown in Fig.(2) based upon Monte-Carlo simulations at 973 K. These

are calculated using the partial bond energies assuming that the cluster retains a fcc lattice arrangement of atoms. Even though these simulations allow the structure of the particle to deviate from the initial cubo-octahedral shape, no such morphology change occurs due to the thermodynamic stability of that arrangement. The one point from the CEM results is also shown. Since the latter allows for continuous deformation of all atomic positions, it provides confidence that the use of the partial bond energy/Monte-Carlo simulation with an fcc lattice is adequate for this system.

Next, consider the Rh_xPd_{1-x} system. The surface energies (in J/m^2) predicted by CEM (MD/MC-CEM) are 1.63 (1.89), 1.74(2.00) and 1.87 (2.18) for Pd(111), Pd(100), Pd(110), respectively.^{4a} Experimental data on surface free energies of polycrystalline samples¹¹ at the metal's melting point and at 298 K can be used to extrapolate to 0 K with the result being $2.17 J/m^2$. The agreement is again excellent. The CEM predictions of the alloy formation energy are 1.5, 1.9 and 1.5 kJ/mole for $x=0.75$, 0.5 and 0.25 respectively. The experimental value¹² at 1575 K is 10 kJ/mole with the difference from 0 K easily made up by variation in heat capacity. The MD/MC-CEM method predicts 2.2, 2.9 and 2.2 kJ/mole, respectively, and is thus quite acceptably accurate.

Results for 201 and 1289 atom clusters are shown in Figs.(3) and (4), respectively. The clusters exhibit increased enrichment of Pd on the surface and a substantial favoring of edge-corner sites at the surface. Thus Pd atoms occupy low coordination sites on the surface. There is only a slight temperature dependence of the enrichment between 600 K and 1000 K.

In the Ni_xPd_{1-x} and Rh_xNi_{1-x} clusters (not shown), the metal segregating to the surface is Pd for the former and Ni for the latter. From these and other systems, a few general statements can be made: 1/ the metal with the smallest surface energy segregates to the lowest coordination sites first, then to other low coordination sites; 2/ an increase in temperature drives the mixing and thus decreases the degree of segregation; and, 3/ as the size of the cluster increases, the surface-segregating metal populates the entire surface at lower total concentration.

Experimental verification of these predictions is problematic. Only surface composition measurements have been attempted leaving site population and micromixing properties to speculation. The standard surface science tools such as Auger electron spectroscopy (AES) are not feasible due to the very nature of the particles. In addition, traditional methods of estimating surface composition using selective chemisorption are known to significantly perturb these bimetallic systems.⁵ In certain simple systems a combination of 1H NMR and hydrogen chemisorption have indicated the predictions give reasonable results.¹³ We can apply the predictions to low-index plane simulations that are more easily verified experimentally, however. The fcc(111) surface of $Rh_{0.9}Pt_{0.1}$ was simulated with the partial bond energy/Monte Carlo method in the same manner as the 201 atom particle discussed above yielding the results in Fig.(5). Recently, Fisher and co-workers have used AES and ion scattering spectroscopy to determine that the surface composition of this system is $\approx 70\%$ Rh in the 1200 K temperature range,¹⁴ which is in good agreement with our predictions.

Acknowledgement

This work was supported by the Advanced Industrial Concepts Division of the U.S. Department of Energy through the Ames Laboratory, which is operated for the U.S. DOE by Iowa State University under Contract No. W-7405-Eng-82. The more extensive CEM calculations were performed on the nCUBE 2 hypercube at two different sites: 1) the Scalable Computing Laboratory, Ames Laboratory; 2) the Massively Parallel Computational Research Laboratory, Sandia National Laboratory at Albuquerque.

References

1. J. H. Sinfelt, Bimetallic Catalysts: Discoveries, Concepts and Applications, John Wiley & Sons, (1983).
2. a) J. D. Kress and A. E. DePristo, *J. Chem. Phys.* **88**, 2596 (1988);
b) J. D. Kress, M. S. Stave and A. E. DePristo, *J. Phys. Chem.* **93**, 1556 (1989);
c) M. S. Stave, D. E. Sanders, T. J. Raeker and A. E. DePristo, *J. Chem. Phys.* **93**, 4413 (1990);
d) T. J. Raeker and A.E. DePristo, *Int. Rev. Phys. Chem.* **10**, 1 (1991).
3. a) T. J. Raeker, D. E. Sanders and A. E. DePristo, *J. Vac. Sci. Tech.* **A8**, 3531 (1990);
b) T. J. Raeker and A. E. DePristo, *Surf. Sci.* **248**, 134 (1991);
c) T. J. Raeker and A. E. DePristo, "Alloy formation energetics and dynamics in the Ni/Cu(100) and Ni/Cu(111) systems," *J. Vac. Sci. Tech.* **A** (in press, 11/91).
4. a) S. B. Sinnott, M. S. Stave, T. J. Raeker and A. E. DePristo, *Phys. Rev. B* **44**, 8927 (1991);
b) D. E. Sanders, D. M. Halstead and A. E. DePristo, "Metal/metal homo-epitaxy on FCC(111) and FCC(001) surfaces: deposition and scattering from small islands," *J. Vac. Sci. Tech.* **A** (in press, 12/91).
5. T. S. King, "Bond Breaking and Chemical Thermodynamic Models of Surface Segregation," in Surface Segregation Phenomena, eds. P. A. Dowben and A. Miller, CRC Press (1990).
6. X. Wu, S. Bhatia and T. S. King, "Characterization of Small Metal Particles," *J. Vac. Sci. Tech.* **A** (in press).
7. J. K. Strohl and T. S. King, *J. Catal.* **118**, 53 (1989).
8. C. L. Liu, J. M. Cohen, J. B. Adams and A. F. Voter, *Surf. Sci.* **253**, 334 (1991).
9. a) M. S. Daw and M. I. Baskes, *Phys. Rev. B* **29**, 6443 (1984);
b) S. M. Foiles, M. I. Baskes and M. S. Daw, *Phys. Rev. B* **33**, 7983 (1986);
c) T. Ning, Q. Yu and Y. Ye, *Surf. Sci.* **206**, L857 (1988);
d) M. S. Daw, *Phys. Rev. B* **39**, 7441 (1989).
10. T. J. Raeker, L. Yang, A. M. Schoeb, X. Wu, T. S. King and A. E. DePristo, (to be submitted).
11. L. Z. Mezey and J. Giber, *Jap. J. App. Phys.* **21**, 1569 (1982).
12. R. Hultgren, P. D. Desai, D. T. Hawkins, M. Gleiser, and K. K. Kelley, Selected Values of the Thermodynamic Properties of Binary Alloys (American Society for Metals, Metals Park, OH, 1973).
13. X. Wu, B. C. Gerstein and T. S. King, *J. Catal.* **121**, 271 (1990).
14. a) G. B. Fisher and C. L. DiMaggio, *Surf. Sci.* (submitted);
b) D. D. Beck, C. L. DiMaggio and G. B. Fisher (personal communication).

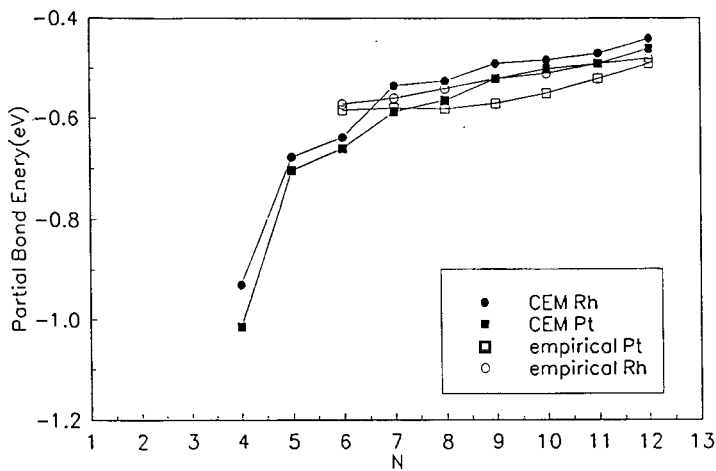


Fig. 1 Partial bond energies for Pt and Rh as determined from CEM calculations and also from previous work using a quadratic form (in N) fit to surface energies.

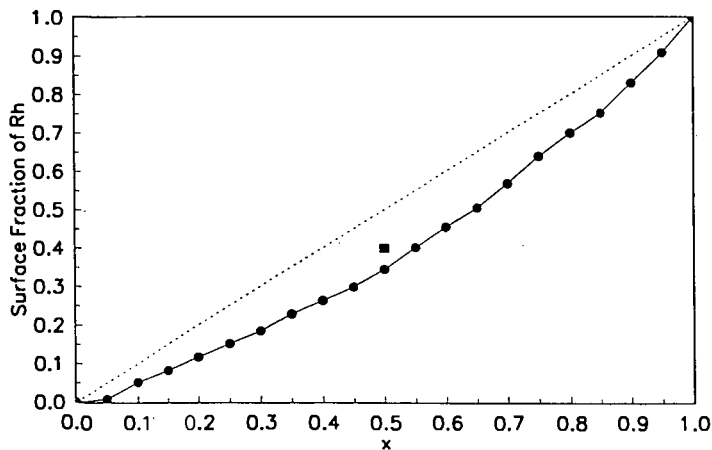


Fig. 2 Surface fraction of Rh in $\text{Rh}_x\text{Pt}_{1-x}$ clusters with 201 total atoms as predicted by the partial bond energy model at 973 K. A single point for $x=0.5$ (■) is shown based upon a full CEM simulation at 600 K. The dotted line separates enrichment (above) and depletion (below) regions.

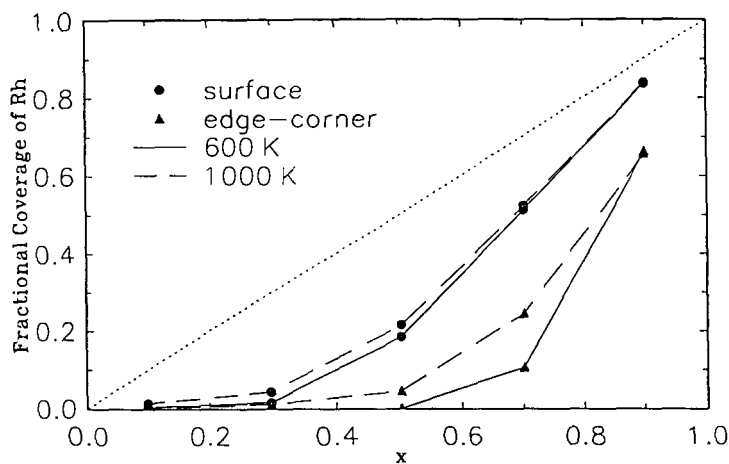


Fig. 3 Fractional coverage of Rh at surface and edge-corner sites in $\text{Rh}_x\text{Pd}_{1-x}$ clusters with 201 total atoms as predicted by the MD/MC-CEM model.

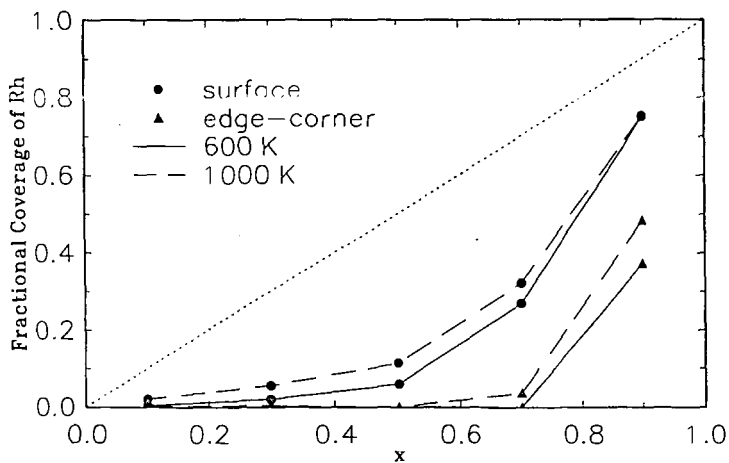


Fig. 4 Same as Fig.(3) but for 1289 total atoms.

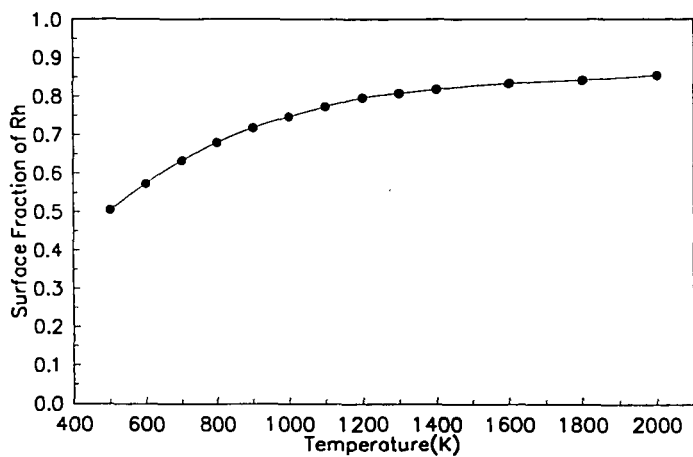


Fig. 5 Surface fraction of Rh in Rh_{0.9}Pt_{0.1}(111) as predicted by the partial bond energy model.

MOLECULAR DESIGN OF SUBSTRATE BINDING SITES

John A. Shelnut, J. David Hobbs

Fuel Science Division 6211
Sandia National Laboratories
Albuquerque, NM 87185

Keywords: Molecular modeling, catalysis, porphyrin

ABSTRACT

Computer-aided molecular design methods were used to tailor binding sites for small substrate molecules, including CO₂ and methane. The goal is to design a cavity, adjacent to a catalytic metal center, into which the substrate will selectively bind through only non-bonding interactions with the groups lining the binding pocket. Porphyrins are used as a basic molecular structure, with various substituents added to construct the binding pocket. The conformations of these highly-substituted porphyrins are predicted using molecular mechanics calculations with a force field that gives accurate predictions for metalloporphyrins (Shelnutt, *et al.*, *J. Am. Chem. Soc.* **1991**, *113*, 4077). Dynamics and energy-minimization calculations of substrate molecules bound to the cavity indicate high substrate binding affinity. The size, shape, and charge-distribution of groups surrounding the cavity provide molecular selectivity. Specifically, calculated binding energies of methane, benzene, dichloromethane, CO₂, and chloroform vary by about 10 kcal/mol for metal octaethyl-tetraethylporphyrins (OETPPs) with chloroform, dichloromethane, and CO₂ having the highest affinities and with methane and benzene having the lowest. Significantly, a solvent molecule is found in the cavity in the X-ray structures of Co- and CuOETPP crystals obtained from dichloromethane.

INTRODUCTION

We have set for ourselves the ambitious goal of designing and synthesizing molecules with a high affinity binding site for a given substrate molecule. Preferably, the molecule containing the substrate binding cavity would also possess some additional chemical functionality, such as a catalytic center at which the substrate would be converted to a useful product. Because over 70 metals in various oxidation states can be incorporated into the porphyrin macrocycle and because of the high degree of variability in the peripheral substituents, we have chosen the metalloporphyrins as a foundation for construction of the required binding site. By using the porphyrin ligand, we gain considerable freedom both in the choice of catalytic metal at its center and in the selection of peripheral substituents used to construct the binding cavity of the chosen substrate molecule.

Our initial goal is to construct a porphyrin with a substrate binding pocket for which only non-bonding forces contribute to the selective binding of the substrate to the active site. The inclusion of such a cavity gives several potential benefits. These benefits include (1) increased affinity for the substrate and decreased product affinity, (2) enhanced selectivity for a particular substrate molecule, (3) enhanced regioselectivity of the reaction, (4) lower catalyst self-destruction rates and increased catalyst stability, (5) product slate selectivity resulting from trapping of radical intermediates for recombination, and (6) enhanced reactivity from molecular orientational and conformational lowering of transition states, to name a few. All of these benefits of a substrate binding pocket are realized to one degree or another in naturally occurring biological catalysts called enzymes, particularly for the metalloporphyrin-containing enzymes. These enzymes, for example cytochrome P₄₅₀, methylreductase, and the photosynthetic reaction center, catalyze many important energy-related chemical or photochemical reactions. Thus, computer-modeling studies of these enzymes give many important clues to the structural features that might be engineered into our designed catalyst. These features include (1) a catalytic metal ion, (2) appropriate electronic properties for the ligands of the metal, (3) complementary size and shape for the substrate binding pocket, (4) suitable properties like hydrophobicity and charge distribution for the groups lining the pocket, and (5) molecular rigidity of the cavity.

The molecular rigidity of the cavity results in enhanced substrate binding affinity, an

especially important asset for catalytic conversion of small gaseous substrate molecules like CO₂ and methane. Because the rigid binding pocket is present even in the absence of the substrate molecule, enzyme studies show that the 'hole' in the catalyst contributes (about 2 kcal/mol) to the binding energy (for each methylene-group-sized unit) of the substrate molecule through the dispersion energy contribution to the interaction with the bound substrate. In the example of an enzyme and its alkane substrate in water, two unfavorable hydrophobic interfaces result, one from the water molecules filling the hydrophobic pocket and another from the alkane dissolved in the solvent; these unfavorable hydrophobic interactions are removed when the substrate binds to the preformed pocket, accounting for about 3 kcal/mol for a methylene-sized molecular unit. Electrostatic forces also enhance the binding energy. After the rigidity of the cavity is insured, energy contributions to the binding energy of the substrate molecule can be optimized by careful design of the binding cavity of our tailored enzyme analog.

The molecular rigidity of the binding pocket possessed by the enzymes has been one of the most difficult structural features to mimic in our metalloporphyrin-based enzyme analogs. However, by using so-called highly substituted porphyrins we have been able to engineer the required molecular rigidity into our designed catalysts. Using a molecular model based on a porphyrin normal coordinate analysis, we found that the porphyrin ring, when maximally substituted at the periphery with non-hydrogen substituent groups, was rigidly distorted into a saddle shaped conformation. Furthermore, in this distorted geometry the substituents at the β -pyrrole carbons form a binding pocket of a size and shape suitable for binding small molecules like CO₂ and light alkanes. And, by lining the pocket with groups with properties complementary to the substrate, we could promote substrate binding to the pocket for times on the order of nanoseconds (in molecular dynamics calculations at 300 °K in vacuum).

Many of the designed catalysts have been synthesized and subjected to experimental structural studies. The calculated conformations of the designed catalysts have been verified by X-ray crystallography, NMR spectroscopy, UV-visible absorption spectroscopy, and resonance Raman spectroscopy.¹⁻³

Evidence of substrate binding is found in the X-ray crystal structures of the cobalt and copper derivatives of octaethyl-tetraphenylporphyrin. As described below, small solvent molecules are observed in the substrate binding cavity in X-ray crystal structures of this highly-substituted metalloporphyrin.

MATERIALS AND METHODS

Cobalt(II) and copper(II) octaethyltetraphenylporphyrin (OETPP) were synthesized as described previously.² The X-ray crystal structures were reported previously,² however the location of solvent molecules in the crystals was not discussed. Views of the packing of porphyrin molecules in the crystal are shown in Figures and were generated on an Evans&Sutherland PS390 graphics workstation. One of two crystallographically distinct solvent molecules is located in the cavity as shown (Figures 2 and 3).

Molecular modeling calculations were performed on a Personal Iris 4D35 workstation using BIOGRAF software from Molecular Simulations, Inc. The calculations were carried out as described previously for a series of nickel porphyrins.² The force field is the same as that reported earlier for nickel(II) porphyrins,² but extended to include other metal ions including Co(II) and Cu(II).³ This force field has been successful in predicting porphyrin conformations that agree well with X-ray crystal structures.^{2,3} Parameters for the oxygen atoms in CO₂ and for the Cl atoms in the halogenated methanes were taken from the DREIDING force field.⁴ Partial atomic charges were assigned to the porphyrin and solvent molecules by the method of charge equilibration.^{4,5} Minimizations were carried out for several initial orientations of the substrate molecule, because of the many local minima resulting from different substrate orientations in the binding pocket.

RESULTS AND DISCUSSION

Figure 1 shows the energy-minimized structure of nickel(II) octapropyl-tetraphenylporphyrin (NiOPTPP) with CO₂ bound in one of the grooves generated by four of the quasi-axial β -pyrrole ethyl substituents. Clearly, CO₂ fits nicely in the elongated cavity of the catalyst, so we decided to evaluate the selectivity of the cavity for a variety of small substrate molecules.

Tables I-III summarize the results of molecular mechanics calculations for the binding of various small molecules, including CO₂, methane, benzene, dichloromethane, and chloroform, to the elongated cavity. The relative binding energies are seen to vary over several kcal/mole, depending

primarily on the size of the substrate and distribution of charge in the substrate molecule. In the model, van der Waals interactions and electrostatic interactions between the substrate molecule and the designed porphyrin catalyst are the only forces that contribute to the binding energy. Benzene binds most weakly because the partial charges on the atoms are small. The chlorinated methanes bind most strongly because the highly electronegative chlorine atoms result in large partial charges on the substrate atoms which interact strongly with complementary charges on the catalyst. In particular, the interactions between the electronegative oxygen (or chlorine) atoms of the substrate and the nearby hydrogen atoms of the ethyl groups of the catalyst are important. In our calculation the electrostatic energy falls off as $1/r^2$, making the interactions with the closest atoms most significant. The $1/r^2$ -dependence is used to mimic the presence of a solvent in a crude way. The dielectric constant of the solvent is assumed to be 1, represents an organic solvent.

Examination of Tables I and II, for catalysts with well defined cavities (NiOETPP and CuOETPP), shows that the order of binding energies is: $\text{CHCl}_3 > \text{CO}_2 \approx \text{CH}_2\text{Cl}_2 > \text{benzene} > \text{methane}$. The van der Waals contribution to the binding energy varies over the range from 6 to 13 kcal/mole for all substrates, lowest values being for the smallest substrates of the group. The electrostatic contribution is large (2-6 kcal/mole) for the substrates with electronegative atoms and small for the hydrocarbons. The internal energies (bond stretch, angle bend, etc.) adjust to some extent upon substrate binding, particularly the torsions. The cavity is slightly larger for CuOETPP (Table II) than for NiOETPP (Table I), and the larger cavity results in weaker binding of each substrate. This effect is even more in evidence when the ethyl groups are replaced by methyl groups (NiOMTPP, Table III), and the cavity is lost altogether. Then, the binding energies of all substrates (except benzene) decrease.

Clearly, the results in Tables I and II indicate that dichloromethane is expected to have one of the highest affinities for the cavity. Therefore, it is not surprising to find a dichloromethane molecule in the cavity in the X-ray crystal structure of the Co and Cu derivatives of OETPP. Figures 2 and 3 show orthogonal views of two of the CuOETPP molecules in the crystal. Also shown are two equivalent dichloromethane molecules that are located in the cavity. The dichloromethane molecules are not coordinated to the copper(II) ion. Copper is usually four-coordinate, square planar with the porphyrin occupying all four ligand sites. The lack of coordination of the dichloromethane is also clear from the greater than 3-Å distance between the metal and the heavy atoms of the substrate.

The binding site apparently does not have a strong preference for a particular orientation of the bound substrate molecule. We conclude this from the many orientations of the substrate molecule that give rise to structures with energies close to the lowest listed for each substrate in Table I. Two such structures are given for dichloromethane and CO_2 in the Tables. Here too, the X-ray data support a similar conclusion based on the thermal parameters for atoms of the dichloromethane located in the cavity. The isotropic displacement coefficient for the carbon atom of the dichloromethane molecule in the pocket is approximately twice as large as for the average carbon atom of the porphyrin. The isotropic parameters for the chlorines are about four times as large as the average carbon atom. This points to a disordered orientation of the dichloromethane molecule in the cavity. The second crystallographically distinct dichloromethane molecule, which is not located in the pocket, is even more disordered.

Efforts are in progress to measure $^{13}\text{CO}_2$ binding to the iron(III) derivatives of the designed catalysts using ^{13}C -NMR spectroscopy. On the basis of the molecular modeling results we have chosen to carry out the experiments in the solvent benzene, which is less likely to spend time in the cavity. We wish to measure the decrease in the ^{13}C relaxation time (T_1) due to the interaction with the paramagnetic Fe(III) center in FeOETPP, when the porphyrin is added to a solution of benzene saturated with $^{13}\text{CO}_2$. The relaxation time decreases depending on how much time the $^{13}\text{CO}_2$ stays in the vicinity of the paramagnetic center and how close to the center the CO_2 comes. Thus, we expect to find a much larger decrease for FeOETPP, which has a binding cavity for CO_2 , than for Fe octamethyl-tetraphenylporphyrin (FeOMTPP), which is structurally very similar to FeOETPP but lacks a cavity in which CO_2 can bind. From Table III, note that the ordering of substrate binding energies is different when the cavity is lost for CuOMTPP. In particular, the benzene solvent binds more strongly than CO_2 for OMTTPs. Preliminary experiments in collaboration with R. A. Assink support these conclusions.

ACKNOWLEDGEMENTS

This work supported by U. S. Department of Energy Advanced Industrial Concepts Catalysis/Biocatalysis Program and Pittsburgh Energy Technology Center under Contract DE-AC04-76DF00789. We express thanks to C. J. Medforth at the University of California at Davis and R. A. Assink at Sandia National Laboratories for helpful discussions.

REFERENCES

1. Medforth, C. J.; Berber, M. D.; Smith, K. M.; Shelnut, J. A., *Tetrahedron Letts.* **1990**, 31, 3719.
2. Shelnut, J. A.; Medforth, C. J.; Berber, M. D.; Barkigia, K. M.; Smith, K. M., *J. Am. Chem. Soc.* **1991**, 113, 4077.
3. Sparks, L. D.; Medforth, C. J.; Park, M.-S.; Chamberlain, J. R.; Ondrias, M. R.; Senge, M. O.; Smith, K. M.; Shelnut, J. A., *J. Am. Chem. Soc.*, 1992, submitted.
4. Mayo, S. L.; Olafson, B. D.; Goddard III, W. A., *J. Phys. Chem.* **1990**, 94, 8897.
5. Rappe, A. K.; Goddard III, W. A., *J. Phys. Chem.*, to be submitted.

TABLE I. Relative Substrate Binding Energies (kcal/mole) and Distance from Metal to Nearest Substrate Atom (Å) for Ni Octaethyl-Tetraphenylporphyrin.

Substrate	Total E	VDW	ES	Torsion	Angle	Bond	Invers.	Dist.*
methane	7.4	5.8	2.3	-1.9	0.3	0.7	0.0	3.88 C
benzene	10.4	9.6	0.0	0.5	0.2	0.0	0.0	3.37 C
CH ₂ Cl ₂	14.0 12.7	12.1 9.7	2.8 4.4	-2.1 -1.3	0.0 -0.5	1.2 0.4	0.0 0.0	3.17Cl 3.73 C
CO ₂	14.3 13.9	8.9 9.1	5.7 6.1	-0.9 -1.6	0.0 -0.1	0.4 0.4	0.3 0.0	3.43 C 3.20 C
CHCl ₃	17.1	13.0	5.1	-1.9	-0.2	1.2	0.0	3.23Cl

*Distance between the metal and the nearest heavy atom.

TABLE II. Relative Substrate Binding Energies (kcal/mole) and Distance from Metal to Nearest Substrate Atom (Å) for Cu Octaethyl-Tetraphenylporphyrin.

Substrate	Total E	VDW	ES	Torsion	Angle	Bond	Invers.	Dist.*
methane	5.5	4.6	2.0	-1.5	-0.2	0.7	-0.1	3.56 C
benzene	10.0	0.7	10.6	-1.6	-0.1	0.4	0.0	3.56 C
CH ₂ Cl ₂	12.5	7.0	3.8	1.6	-0.2	-0.2	0.4	3.65 C
	11.6	10.7	2.3	-1.3	-0.3	0.2	0.0	3.54Cl
CO ₂	12.8	6.7	5.4	-0.3	0.2	0.7	0.0	3.19 C
	12.7	9.8	7.2	-3.7	-0.8	0.5	-0.5	3.39 C
CHCl ₃	15.2	12.3	5.5	-2.6	-0.3	0.9	-0.6	3.29Cl

*Distance between the metal and the nearest heavy atom.

TABLE III. Relative Substrate Binding Energies (kcal/mole) and Distance from Metal to Nearest Substrate Atom (Å) for Ni Octamethyl-Tetraphenylporphyrin.

Substrate	Total E	VDW	ES	Torsion	Angle	Bond	Invers.	Dist.*
methane	4.4	3.2	1.0	0.1	0.3	-0.1	-0.1	3.48 C
benzene	10.9	10.2	0.1	0.1	0.4	0.2	-0.1	3.85 C
CH ₂ Cl ₂	10.1	8.5	2.2	-0.7	-0.3	0.5	-0.1	3.46 C
	10.1	8.6	2.5	-1.7	0.1	0.7	-0.1	3.57Cl
CO ₂	9.6	7.0	2.9	-0.2	-0.1	0.0	-0.1	3.13 O
	6.8	6.5	0.2	-0.9	-0.1	1.1	-0.1	3.24 C
CHCl ₃	11.9	9.2	3.8	-1.2	-0.4	0.5	-0.1	3.60Cl

*Distance between the metal and the nearest heavy atom.

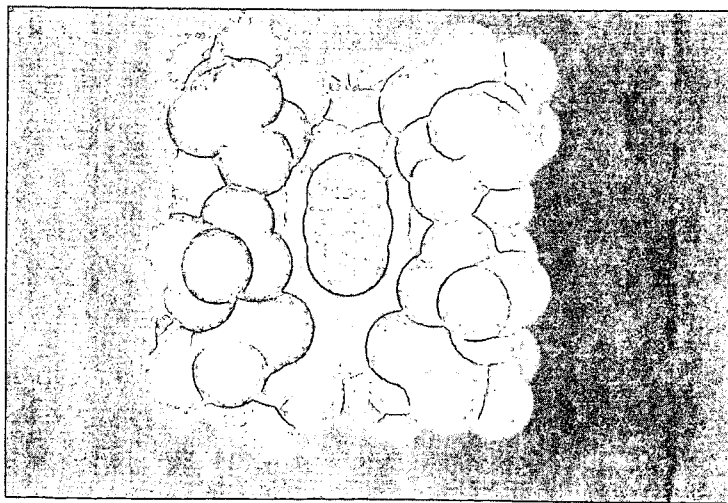
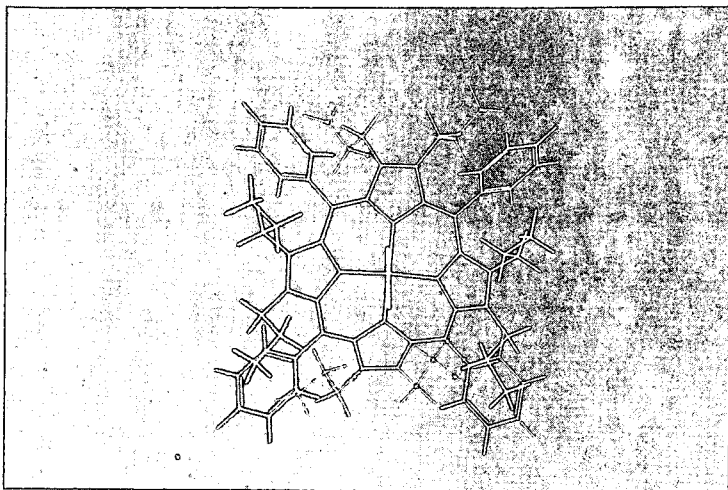
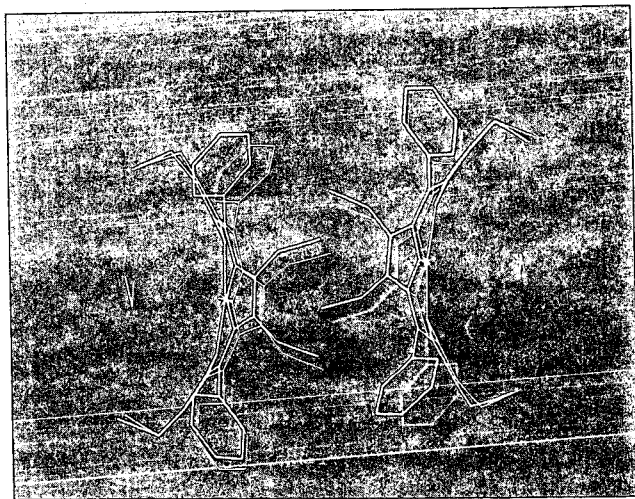
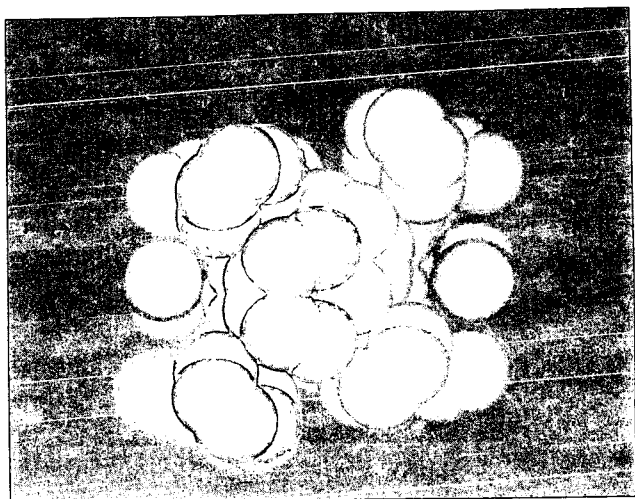


Figure 1. Energy-minimized structure of nickel(II) octapropyl-tetraphenylporphyrin (NiOPTP) showing CO₂ bound in the cavity formed by the porphyrin macrocycle and the quasi-axial ethyl groups. View looking down into the substrate binding cavity of NiOPTP where CO₂ is bound (center).



View of the X-ray crystal structure of copper(II) octaethyl-tetraethylporphyrin (CuOETTP) showing two molecules of CuOETTP and two dichloromethane molecules (top and bottom) in the binding cavity.

Figure 2.

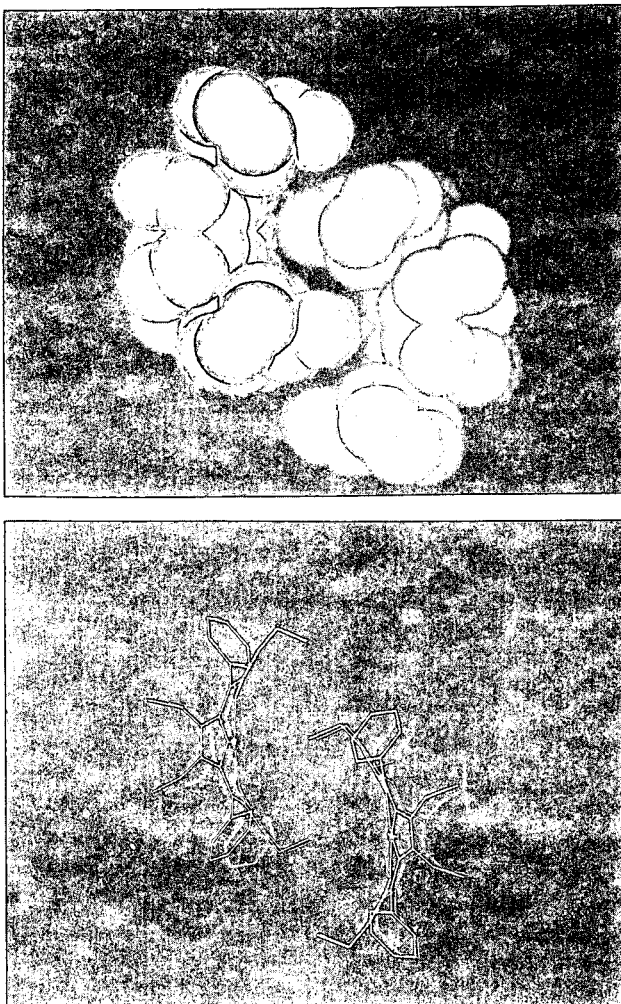


Figure 3. View of the X-ray crystal structure of copper(II) octaethyl-tetraphenylporphyrin (CuOETPP) showing two molecules of CuOETPP and two dichloromethane molecules (top and bottom) in the binding cavity. View is orthogonal to that of Figure 2.

**THE SYNTHESIS AND CHARACTERIZATION OF NEW COPPER
COORDINATION COMPLEXES CONTAINING AN ASYMMETRIC
COORDINATING CHELATE LIGAND: APPLICATION TO ENZYME ACTIVE
SITE MODELING ***

M.W. Droege,¹ J.H. Satcher, Jr.,¹ R.A. Reibold,¹ T.J.R. Weakely²

¹Lawrence Livermore National Laboratory, PO Box 808, Livermore, Ca., 94550

²Dept of Chemistry-University of Oregon, Eugene, OR., 97403

Keywords: *Asymmetric coordination, binuclear complex, methane monooxygenase*

ABSTRACT

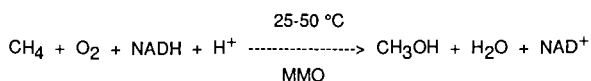
A new class of ligand which produces a binuclear metal complex with coordination asymmetry has been designed and synthesized. A binuclear copper complex has been prepared and characterized including a single crystal x-ray structure analysis. The structure reveals that one copper is 5-coordinate (distorted square pyramidal) while the other copper is only 4-coordinate (distorted square planar) and are separated by an endogenous μ -alkoxo oxygen and a bridging acetate. Although this structural type of chelator has been found in biological systems, it has not been previously described for inorganic coordination complexes prepared by design. It is anticipated that this ligand and derivatives of it will play an important role in mimicking chemical reactivity of enzyme active sites that function by substrate interaction at only one metal of a multimetal active site.

INTRODUCTION

The catalytic oxidation of light hydrocarbons, especially methane derived from natural gas, is an important research area attracting considerable attention. The potential for natural gas (methane) processing will depend on the development of catalyzed routes directly converting methane to higher valued products (heavier hydrocarbons, olefins, and alcohols). However, methane is chemically quite inert and has not proved easy to convert to liquid hydrocarbons. As a result, no technologies are currently available to process methane economically. It is well-known that a select group of aerobic soil/water bacteria called methanotrophs can efficiently and

*Work performed under the auspices of the U.S. Department of Energy by the Lawrence Livermore National laboratory under Contract No. W-7405-ENG-48.

selectively utilize methane as the sole source of their energy and carbon for cellular growth.¹ The first reaction in this metabolic pathway is catalyzed by the enzyme methane monooxygenase (MMO) forming methanol:



Methanol is a technologically important product from this partial oxidation of methane since it can be easily converted to liquid hydrocarbon transportation fuels, used directly as a liquid fuel itself, or serve as a feedstock for fine chemicals production.

Microorganisms can produce MMO in two distinct forms: a membrane-bound particulate form or a discrete soluble form. The soluble form consist of three main proteins: A, B, and C. Protein A is an iron-containing oxygenase that reacts with methane, producing methanol,² and is therefore the focus of our work. Spectroscopic and thermodynamic studies have postulated that the metals in Protein A occur in a binuclear iron center and function as the active site for methane oxidation.^{3,4,5} Although some of the details vary, the general description of the iron site in Protein A is a binuclear cluster containing some type of μ -oxo ligand between the iron atoms. The remaining ligands (derived from adjacent amino acid residues) coordinate to the metals through nitrogen or oxygen and the Fe-Fe distance is between 3.0-3.5 Å. Compared to the soluble form of MMO the particulate form is poorly characterized and is thought to contain copper ions at the active site. This form is also active in methane oxidation in the biological system.⁶

Our work centers on the synthesis and characterization of inorganic/organic chemical models of the active site of MMO (both particulate and soluble). We have focused on the synthesis of an unsymmetrical, binuclear chelating ligand possessing an alkoxy group that can serve as a bridging μ -oxo ligand. The advantage of such a ligand system is twofold: (a) metal complexes of an asymmetric binucleating ligand will provide coordinative unsaturation at only one metal resulting in focused substrate reactivity at that site and (b) a single ligand with binuclear coordination provides a more robust environment for metal oxidation state changes and accompanying chemical reactivity.

We report here the synthesis of a prototype asymmetrical binuclear chelating ligand, its reactivity with copper ion, and characterization of two new copper chelate complexes. This work provides the first proof-of-concept for the formation of a binuclear complex with different coordination at each metal ion. Such complexes are relevant to the development of model systems for the active site of MMO.

EXPERIMENTAL

The synthesis of the chelating ligand HMeL obtained by a five step procedure in ~35% overall yield is outlined in scheme 1. The synthesis of copper complexes of this ligand are described below.

(N,N,N'-tris-((N-methyl)-2-benzoimidazolylmethyl)-N'-methyl-1,3-diamino-2-propionato) copper(II) perchlorate [CuHMeL(ClO₄)₂·CH₃CN (1). A solution of 1.00g (1.86 mmol) of HMeL in 15 mL methanol was treated with a solution of 0.688g Cu(ClO₄)₂·xH₂O (17.2% Cu, 1.86 mmol Cu²⁺) in 15 mL methanol with stirring. A blue precipitate forms immediately on addition of copper solution and the mixture was allowed to stir at room temperature for 10 minutes. The resulting mixture was cooled at -20°C for ~1 hr, the blue solid collected on a glass frit (pale green filtrate), washed with 10-15 ml cold methanol and dried under vacuum at 25°C. Crude yield was 1.3256g of blue-green solid. The dried solid was dissolved in 75 mL hot acetonitrile, filtered hot, and cooled. X-ray quality crystals were obtained by vapor diffusion of ether into this solution. The blue-green crystals were collected on a frit and vacuum dried (83% yield). Anal. Calcd. for C₃₃H₃₉Cl₂CuN₉O₉: C, 47.18; H, 4.68; N, 15.00. Found: C, 47.07; H, 4.85; N, 14.73.

(μ-O,O'-acetato)(N,N,N'-tris-((N-methyl)-2-benzoimidazolylmethyl)-N'-methyl-1,3-diamino-2-propionato)dicationicopper(II,II) bisperchlorate [Cu₂MeL(OAc)(ClO₄)₂·2H₂O (2).

(a) A solution of 1.00g of HMeL (1.86 mmol) and 0.507g sodium acetate trihydrate (3.72 mmol) in 15 mL of methanol was treated with 1.377g Cu(ClO₄)₂·xH₂O (17.2% Cu, 3.72 mmol Cu²⁺) in 15 mL methanol with stirring. A light blue precipitate forms initially and is quickly replaced (~30 sec) by a deep blue solid. The mixture was stirred for 30 min. at room temperature and then cooled at -20°C overnight. The solid was collected on a glass frit, washed with 10mL of cold methanol, and air dried to yield 1.703g of sky-blue powder. Further purification was achieved by vapor diffusion of ether into 50 mL of an acetonitrile solution of this solid to yield dark blue crystals (90.3% yield). Anal. Calcd. for C₃₃H₄₂Cl₂Cu₂N₈O₁₃: C, 41.43; H, 4.64; N, 11.71. Found: C, 41.34; H, 4.64; N, 11.13. (b) A 0.1036g (0.125 mmol) sample of (1) was placed in 10 mL of methanol to produce a pale blue-green solution and solid. To this suspension 0.046g of Cu(ClO₄)₂·xH₂O (0.125 mmol) followed by 0.034g sodium acetate trihydrate (0.25 mmol) were added sequentially as solids. The mixture was warmed to 50°C and stirred for 30 minutes. The solid was collected and washed with cold methanol, and recrystallized by vapor diffusion of ether in acetonitrile to yield dark blue crystals of (2).

RESULTS AND DISCUSSION

Scheme 1 shows the synthetic route for the prototype binuclear chelating ligand, HMeL. Elemental analysis and NMR studies confirm the composition and structure of the ligand. It possesses a hydroxy functionality that could serve as a bridging alkoxo group and aliphatic and

aromatic nitrogen coordination groups (benzimidazole). Using the C-OH bond as a bisecting line in this molecule, it is clear that the ligand has the potential to coordinate two metal ions in different environments. One half of the ligand provides three coordination sites (2 nitrogens and 1 bridging oxygen) while the other half provides four coordination sites (3 nitrogens and 1 bridging oxygen).

Reactions with copper ion demonstrate that the ligand is a potent chelating agent. Blue or blue-green colored complexes are formed rapidly in the presence of copper(II). The complexes are synthesized by stoichiometric reactions in methanol using hydrated metal salts. Characterization by elemental analysis and single crystal x-ray crystallography show that either mononuclear or binuclear complexes are obtained. For a metal-to-ligand ratio of 1:1 a mononuclear complex is obtained (Figure 1). The structure of the complex shows a distorted, trigonal bipyramidal coordination environment around Cu with five Cu-N bonds (average Cu-N distance $\sim 2 \text{ \AA}$). In this case, the hydroxo functionality does not coordinate to the metal and in the structure is located remote from the metal. On the other hand, with a metal-to-ligand ratio of 2:1 and in the presence of 2 equivalents of sodium acetate, a binuclear complex is formed (Figure 2). The structure shows that the ligand has chelated two copper ions, that the copper ions share the alkoxo oxygen (bridging μ -oxo), and that a coordinated acetate ion bridges the two metals. As a result, one Cu ion is coordinatively saturated (5-coordinate distorted trigonal pyramidal) while the other Cu is only four coordinate (distorted square pyramid). The mixed oxygen, nitrogen ligation have average Cu-N(O) distances of $\sim 2 \text{ \AA}$ typical of Cu(II) coordination complexes. The role of acetate in this reaction is both to serve as a coordinating bridge between the two copper sites and as a general base that assists in deprotonation of the organic hydroxo group forming the charged alkoxo bridging species. Interestingly, the crystal structure shows that in the solid-state an oxygen from one of the ClO_4^- counterions is weakly bound to the 4-coordinate Cu ion (about 2.6 \AA away) suggesting that this Cu is coordinatively unsaturated and that there is a potential 5th site for binding. Initial attempts to demonstrate this binding site have been successful and an azido bridged binuclear Cu complex has been prepared and isolated.⁷ It appears that complexes of this type can show selective reactivity at one metal site. Such behavior is a key requirement for bioinorganic mimics of the MMO active site.

CONCLUSIONS

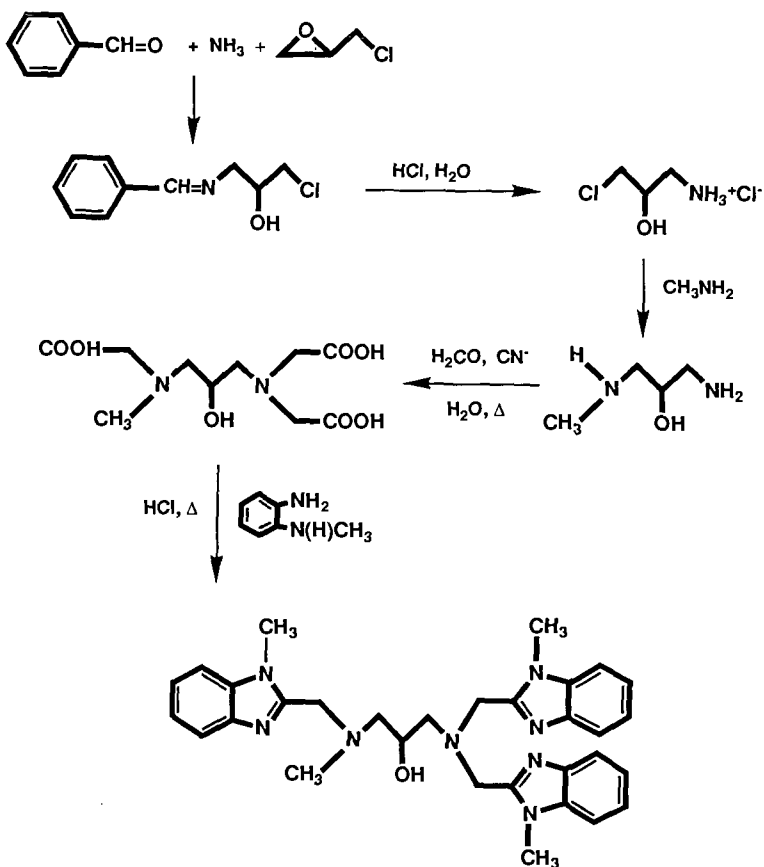
A binuclear, unsymmetric coordinating ligand that is an effective metal chelator has been designed and prepared. The new ligand has been shown to react rapidly with copper(II) forming a variety of copper coordination complexes. The binuclear complex is of significant interest since it represents proof-of-principle for the development of coordinatively asymmetric, binuclear metal chelate complexes. Although this structural type of chelator now appears to be common in biological systems, it has not been previously described for inorganic coordination chemistry. It is

expected that this ligand and derivatives of it will play an important role in the development of bioinorganic complexes that aim to mimic enzyme active sites that function by substrate interaction at only one metal site of a multimetal active site.

Work performed under the auspices of the US Department of Energy by the Lawrence Livermore National Laboratory under contract No. W-7405-ENG-48

REFERENCES

1. Dalton, H. *Adv. Appl. Microbiol.* **1980**, *26*, 71-87.
2. (a) Woodland, M.P.; Dalton, H. *J. Biol. Chem.* **1984**, *259*, 53-59. (b) Green, J.; Dalton, H. *J. Biol. Chem.* **1985**, *260*, 15795-15801. (c) Fox, B.G.; Froland, W.A.; Dege, J.E.; Lipscomb, J.D. *J. Biol. Chem.* **1989**, *264*, 10023-10033.
3. (a) Woodland, M.P.; Patil, D.S.; Cammack, R.; Dalton, H. *Biochim. Biophys. Acta* **1986**, *873*, 237-242. (b) Fox, B.G.; Surerus, K.K.; Munck, E.; Lipscomb, J.D. *J. Biol. Chem.* **1988**, *263*, 10553-10556.
4. Prince, R.C.; George, G.N.; Savas, J.C.; Cramer, S.P.; Patel, R.N. *Biochim. Biophys. Acta* **1988**, *952*, 220-229.
5. Ericson, A.; Hedman, B.; Hodgson, K.O.; Green, J.; Dalton, H.; Bentsen, J.G.; Beer, R.H.; Lippard, S.J. *J. Am. Chem. Soc.* **1988**, *110*, 2330-2332.
6. (a) Stanley, S.H.; Prior, S.D.; Leak, D.J.; Dalton, J. *Biotechnol. Lett.* **1983**, *5*, 487. (b) Park, S., Hanna, M.L., Taylor, R.T., Droege, M.W. *Biotechnology and Bioengineering* **1991**, *38*, 423-433.
7. Droege, M.W.; Satcher, J.H., Jr.; Weakley, T.J.R. Unpublished results.



Scheme 1. Reaction pathway producing chelating ligand [HMeL].

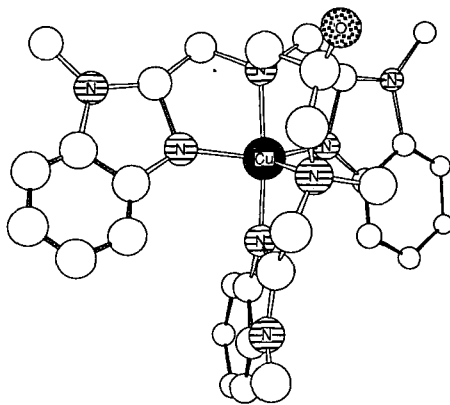


Figure 1. Structure of mononuclear Cu(II) complex (1). Open circles represent carbon atoms. Hydrogen atoms not shown for clarity.

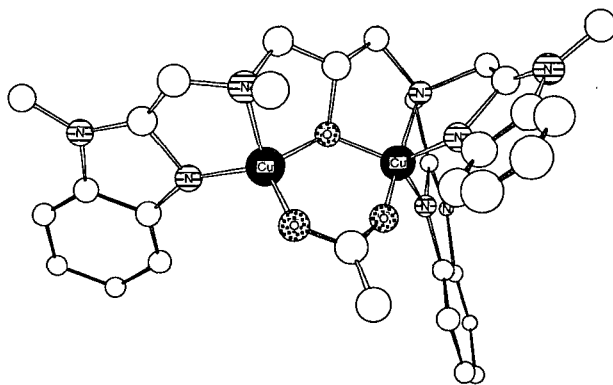


Figure 2. Structure of binuclear Cu(II) complex (2). Open circles represent carbon atoms. Hydrogen atoms not shown for clarity.

SUPPORT EFFECTS ON PALLADIUM CATALYSTS FOR METHANOL FUEL APPLICATIONS

Todd F. Brewer and Martin A. Abraham
Department of Chemical Engineering
The University of Tulsa
Tulsa, OK 74104

Ronald G. Silver
Allied Signal, Inc.
P.O. Box 580970
Tulsa, OK 74158

ABSTRACT

Methanol, formaldehyde, carbon monoxide, and propylene conversion were examined in a laboratory flow reactor over three base-metal containing alumina-supported palladium (Pd) catalysts in addition to Pd on γ -alumina catalyst. The base metals were cerium, barium, and a combination of the two. Experiments were performed to determine the effect of air to fuel ratio on lightoff temperatures of various feed components for the base-metal catalysts as compared to Pd on γ -alumina. For a vehicle operating at fuel-rich or stoichiometric conditions, the cerium containing catalyst gave the best overall performance among those tested. However, at lean conditions, all the catalysts had similar performance.

Keywords: Methanol Oxidation, Palladium Catalyst, Base Metals

INTRODUCTION

Methanol is a strong candidate as an alternative fuel to gasoline. Since methanol is essentially free of contaminants such as lead and sulfur, it has an advantage over gasoline in minimizing the poisoning of catalysts used for emissions control. In addition, methanol exhaust does not contain many of the hydrocarbon species present in gasoline exhaust. Methanol exhaust is composed primarily of unburned methanol, formaldehyde, carbon dioxide, and small amounts of hydrocarbons generated when methanol is used as a mixture with gasoline. The major components that are cause for concern are the photochemically active formaldehyde and the unburned methanol.

Unburned methanol is of particular importance during cold-start conditions where a vehicle

usually operates under fuel-rich conditions to improve driveability. Methanol levels in the exhaust during cold-start conditions can be as high as 0.9 volume percent as compared to 0.04 volume percent during normal operation (McCabe, et al., 1990). With the passage of the Clean Air Act, further tightened restrictions on exhaust emissions have resulted in extensive research on the design of catalysts that will reduce emissions from a methanol-fueled vehicle.

McCabe and coworkers (McCabe, et al., 1986) investigated the effect of feed stream composition and reactor temperature on methanol oxidation. Among the catalysts tested, rhodium (Rh), silver (Ag), and copper (Cu) were found to be much less active than either platinum (Pt) or palladium (Pd) (McCabe, et al., 1986). However, the presence of carbon monoxide had

little effect on the oxidation of methanol over these catalysts, while significantly affecting the Pt and Pd catalysts and raising the lightoff temperature for methanol over both catalysts. As a consequence, low temperature methanol oxidation activities of the Ag and Cu catalysts were as good or better than those of Pt or Pd in the presence of carbon monoxide (CO). This is consistent with weak chemisorption of CO compared to methanol on Ag and Cu surfaces, as observed in previous work (Ryberg, 1982; Madix, 1980). Also, the Ag displayed a high selectivity to complete oxidation; in particular, the Ag catalyst provided the lowest formaldehyde yield of all catalysts (McCabe, et al., 1986).

Additional studies by McCabe, et al., (1986) have investigated the kinetics of methanol oxidation on a Pt wire in a flow reactor at low ($3e-4$ atm) pressure. The proposed mechanism involves a major pathway responsible for approximately 99 percent of methanol oxidation and a minor pathway that accounts for the remaining 1 percent. The proposed mechanism is illustrated in Figure 1.

Automotive catalysts for gasoline powered vehicles generally include palladium or platinum. Palladium, which is less expensive than platinum, is subject to poisoning by the sulfur present in gasoline (Kummer, 1986). Methanol fuels generally have very little sulfur, thus Pd only catalysts may be a viable option for alternative-fuel vehicles. In addition, recent experiments have shown extended durability for Pd-only catalysts in engine-aging studies (Summers, et al., 1989). Pd, which is the least expensive noble metal, is also the preferred noble metal for C_1 and C_2 hydrocarbon conversions. Palladium's viability as an option for a methanol-fuel vehicle exhaust catalyst provides the impetus to investigate methanol oxidation over palladium-only catalyst formulations.

This paper presents the results of our experimental evaluation of the performance of two base-metals when incorporated into the washcoat of a palladium monolith catalyst. All results are compared to a palladium-only (Pd) catalyst with an alumina washcoat and no base-metal present. Experiments were conducted in a laboratory flow reactor with a feed gas chosen to simulate exhaust from a

methanol-fuel vehicle. All catalysts were tested fresh as supplied by the manufacturer. The effect of oxygen to fuel ratio on the lightoff temperatures of methanol, formaldehyde, carbon monoxide, and propylene was examined. Within this paper, we report on the performance of each catalyst at varying oxygen and methanol concentration. The effects of variation in the washcoat formulation were determined and analyzed in terms of an appropriate reaction description.

EXPERIMENTAL

Laboratory catalyst evaluations were carried out in a stainless steel flow reactor system shown in Figure 2. Catalyst samples were 1 inch in diameter by 0.5 inch long cylindrical sections of ceramic monolith wrapped with an inert fiberglass paper to eliminate void space between the catalyst and reactor wall. The reactor and process lines were heated with Thermolyne heating tapes, and the reactor temperature was monitored with a type J thermocouple placed against the center of the effluent side of the catalyst. Control of the reactor temperature was achieved with a solid state power controller.

Feed gases were supplied via gas cylinders fitted with pressure regulators and individual gas flow rates were controlled with rotameters. Methanol, formaldehyde, and water were introduced into the feed as liquid and vaporized upon mixing with the heated gas feed. Liquid flow rates were controlled with the combination of a metering valve and a rotameter. The liquid feed was injected into the process stream through a septum port just after the pre-heater of the process gases (Figure 2) and the feed stream passed upward through the catalyst. The pre-heater served to increase the temperature of the feed stream gases sufficiently to insure vaporization of the liquid feed. Temperature at the point of injection of the liquid was measured with a type J thermocouple.

Feed samples were taken at the reactor effluent at low temperature with very little or no conversion (as determined by the partial pressure of CO_2). Conversion of the feed components was measured via off-gas analysis of the effluent stream with a Dycor M200 Series Quadrupole

Gas Analyzer. Data was first taken in analog mode which allowed scanning of a wide (0-100 AMU) mass range to insure there were no unforeseen products, and then in tabular mode, which scans a maximum of twelve pre-selected AMU. Data was recorded in the form of partial pressures and conversion to molar flow rates was accomplished by calibration of each component's response factor with standard gas mixtures. Response factors of the individual gases were measured relative to a standard gas. Deconvolution of the mass spectral data was accomplished using the spectral library supplied by the manufacturer.

Experiments were performed over the range 100-400 °C at varying oxygen and methanol concentration. Data points were taken every 6-7 °C to insure identification of the lightoff temperature within a narrow range. Space velocities in all cases were approximately 13,000 h⁻¹ (volume basis; standard conditions). The Oxygen:Fuel ratio was calculated as :

$$\lambda = \frac{F_{O_2}}{\left(\frac{1}{2}F_{MeOH} + \frac{1}{2}F_{CO} + \frac{1}{2}F_{(C_2H_6)}\right)}$$

where F_i is the molar flow rate of component (i). The oxygen to fuel ratio was manipulated by altering the oxygen content in the feed.

Four different Pd-only catalysts supported on a γ -alumina washcoat on a ceramic monolith were evaluated fresh: 1) Pd-alumina with no base-metal, 2) Pd-alumina with barium, 3) Pd-alumina with cerium, and 4) Pd-alumina with both barium and cerium. All catalysts were supplied by Allied Signal, Inc. Each catalyst sample was preconditioned in a rich ($\lambda < 1$) feed at 350°C for one hour to eliminate any oxide coatings from the surface of the catalyst. All samples were evaluated at 3 different feed compositions : 1) rich feed, $\lambda = 0.75-0.80$, 2) stoichiometric feed, $\lambda = 1$, and 3) lean feed, $\lambda = 1.15-1.20$.

RESULTS

The results are presented as plots of conversion versus reactor temperature, hereafter referred to as lightoff plots. Within this paper, the lightoff temperature is considered the temperature at which 50 percent conversion occurs. The extent of conversion depends on the stoichiometry of the feed stream. All results presented are lightoff plots comparing the performance of the four catalysts tested at one stoichiometry. Methanol conversion is presented at rich, stoichiometric, and lean conditions, while the stoichiometric cases are presented for the other exhaust components; formaldehyde, carbon monoxide, and propylene.

Methanol Conversion

Methanol conversion under rich conditions is indicated as a function of temperature in Figure 3.a. For the palladium-alumina catalyst, conversion increased to approximately 0.2 at 150 °C, then decreased as the temperature increased to 200 °C. At that point, methanol conversion increased dramatically, achieving greater than 0.8 conversion at 250 °C. The addition of cerium led to a substantial decrease in lightoff temperature, and eliminated the low temperature peak in conversion. With cerium present, conversion increased steadily over the temperature range 120 to 200 °C. With barium in place of cerium, a similar effect was noticed, however, the lightoff temperature was shifted nearly 80 °C to higher temperatures compared to Pd on bare alumina. The addition of cerium to the barium containing catalyst had essentially no effect on the lightoff behavior for methanol.

Similar results were observed for stoichiometric feed conditions. As illustrated in Figure 3.b, the palladium-alumina catalyst exhibited slight conversion at approximately 140 °C, prior to increasing sharply at 200 °C. The addition of cerium provided a small decrease in the observed lightoff temperature to 190 °C and again eliminated the low temperature peak in conversion. In this case, the presence of barium increased the low temperature conversion to 0.2 at approximately 140 °C, but increased the lightoff temperature relative to the Pd-alumina

catalyst. Cerium addition to the barium-containing catalyst eliminated the low temperature conversion and decreased the lightoff temperature to approximately 175 °C.

Results for the lean case, indicated in Figure 3.c, illustrate a narrowing of the lightoff temperature range between the four catalysts. The palladium-alumina catalyst displayed a steady increase in conversion to 0.40 as the temperature increased to 190 °C; the low temperature peak phenomenon was not evident in this case. The addition of cerium did not dramatically affect the lightoff temperature, however, the low temperature conversion was diminished compared to the palladium-alumina case. The addition of barium increased the lightoff temperature by approximately 25 °C relative to all other catalysts, and gave the poorest conversion at low temperature. The addition of cerium to the barium-containing catalyst improved the low temperature conversion from 0.05 at approximately 150 °C for the barium-only case to 0.2 for the combined catalyst. In addition, the combined catalyst provided a lower lightoff temperature by about 20 °C than the barium catalyst.

Comparison of methanol conversion as a function of stoichiometry indicates: 1) Under rich conditions, the catalysts containing cerium or cerium and barium exhibited the lowest lightoff temperatures for methanol, 2) In all three cases the barium catalyst gave the highest lightoff temperature, and 3) The combined cerium-barium catalyst exhibited the lowest lightoff temperature under stoichiometric and lean conditions.

Other Exhaust Components

Formaldehyde conversion under stoichiometric conditions is presented as a function of temperature in Figure 4. For the palladium-alumina catalyst, a steady increase in conversion was observed over the temperature range 100-180 °C, followed by a sharper increase to 0.8 conversion at approximately 225 °C. The cerium catalyst exhibited the low temperature conversion peak observed previously with the palladium-alumina catalyst during methanol conversion, yet provided a lightoff temperature that was essentially the same as the alumina catalyst. The barium catalyst again exhibited the

poorest performance, exhibiting lightoff at approximately 250 °C, or 30 °C higher than the other catalysts. Cerium addition to the barium-containing catalyst lowered the lightoff temperature to approximately the same as the palladium-alumina and the cerium catalysts. Formaldehyde conversion did not exceed 90 percent for any of the catalysts.

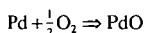
Carbon monoxide (CO) conversion under stoichiometric conditions, shown in Figure 5, was very similar over all four catalysts. Also, the lightoff temperature remained approximately constant between 210 °C and 240 °C, regardless of washcoat composition. Lightoff for CO was much more rapid than was previously noted for methanol, with CO going from near 0% conversion to near 100% conversion in approximately 20 °C. Under stoichiometric conditions complete CO conversion was observed in all catalysts. The combined cerium-barium catalyst yielded the highest lightoff temperature, approximately 25 °C higher than the other catalysts, which all exhibited essentially the same lightoff behavior.

Propylene conversion (Figure 6) displayed many of the same patterns as did the conversion of CO. For this component, as well as CO, the lightoff range narrowed as oxygen content increased. Lightoff temperatures also consistently decreased with increasing oxygen. Propylene exhibited a very narrow temperature range for lightoff, similar to that observed for CO. Conversion increased from essentially 0% to approximately 100% in about 20 °C. Again, the combined cerium-barium catalyst exhibited the highest lightoff temperature of the four catalysts, with 0.5 conversion occurring at approximately 250 °C, as opposed to approximately 220 °C for the palladium-alumina catalyst.

DISCUSSION

The low temperature conversion peak can be interpreted according to previous theory put forth by McCabe, et. al. (1988), for oxidation of formaldehyde over palladium catalyst. In that analysis, it is assumed that the palladium surface is in a reduced state at low temperature conditions but in the oxidized state at higher temperatures. Kinetic analysis of methanol

oxidation over a palladium monolith catalyst has been performed previously (Brewer, and Abraham, 1991) that would seem to support this theory. It may be that the reaction



occurs between 140 and 150 °C. The lower activity of the oxidized surface for oxidation reactions would possibly explain the decrease in catalyst activity in this temperature range. Another explanation could be the presence of two pathways, similar to the mechanism illustrated in Figure 1, where one pathway is favored over a select temperature range and upon passage to sufficiently high temperature a shift back to the major pathway occurs.

The barium catalyst gave the worst performance for methanol oxidation under all conditions. Conversely, catalysts containing cerium consistently were amongst the best-performing catalysts for methanol oxidation. In general, for all catalysts tested in these experiments, an effect of increasing the oxygen concentration was to decrease the lightoff temperature (the exceptions being the lightoff temperatures of 160 °C and 190 °C observed for the cerium-barium and the cerium catalyst under stoichiometric conditions). These observations suggest that cerium enhances the availability of oxygen for the methanol oxidation reaction, whereas barium decreases oxygen availability. As oxygen concentration in the feed increased, and thus its availability for reaction, the influence of cerium was diminished; the inhibition by barium was apparently secondary relative to the enhancement due to cerium.

CONCLUSIONS

Methanol conversion is one of the major topics of concern in methanol-fueled vehicle emissions. Conversions under rich conditions are of particular interest because the vehicles run under rich conditions when they are first started, which is also when catalyst temperatures are low. The cerium catalyst and the combined cerium-barium catalyst displayed the best performance in the conversion of methanol under

rich conditions, the combined Ce-Ba catalyst was best under stoichiometric conditions, and all four catalysts were roughly equal under lean conditions. The barium catalyst generally provided the highest lightoff temperatures of the catalysts tested, although barium did not seem to hinder the performance of the combined cerium-barium catalyst appreciably.

REFERENCES

- Brewer, T.F.; Abraham, M.A. "Methanol Oxidation over Palladium Monolith Catalyst", submitted for publication, (1991).
- Kummer, J.T., *J. Phys. Chem.*, **90**, 4747, (1986).
- Madix, R.J., in "Advances in Catalysis", Academic Press: New York, (1980).
- McCabe, R.W.; Mitchell, P.J., *J. Phys. Chem.*, **90**, 1428, (1986).
- McCabe, R.W.; Mitchell, P.J., *Applied Catalysis*, **27**, 83, (1986).
- McCabe, R.W.; Mitchell, P.J., *Applied Catalysis*, **44**, 73, (1988).
- Ryberg, C.R., *Phys. Rev. Lett.*, **49**, 1579, (1982).
- Summers, J.C.; White, J.J.; and Williamson; W.B., *SAE Paper #890794*, presented at International Congress and Exposition, (1989).

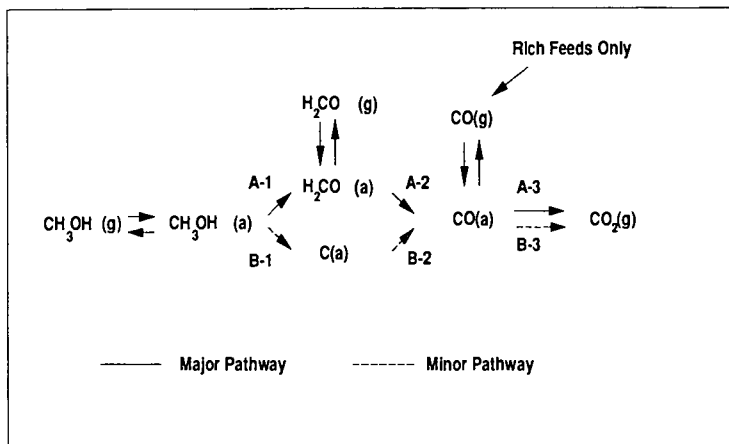


Figure 1: Proposed methanol oxidation pathways (McCabe, et al., 1986). Pathways are simplified. Only carbon-containing species are shown; (a) denotes adsorbed species.

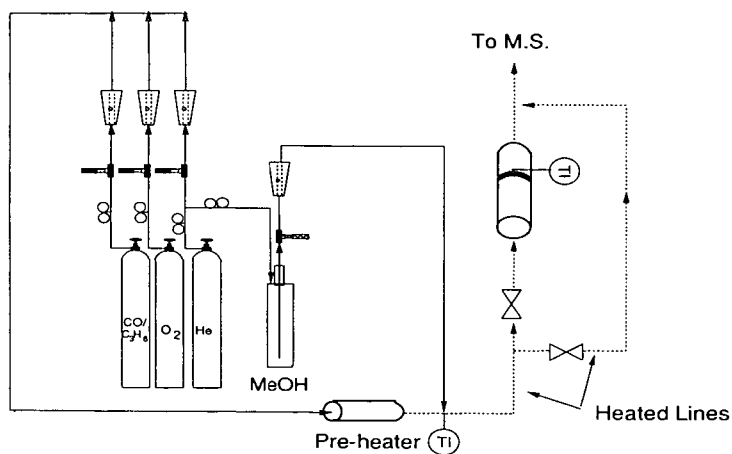


Figure 2: Detailed schematic of experimental apparatus.

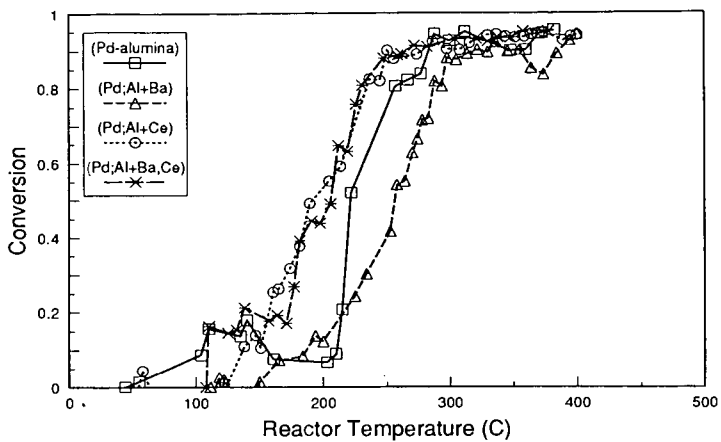


Figure 3.a: Effect of base metal additives on methanol conversion under rich feed conditions ($\lambda < 1$).

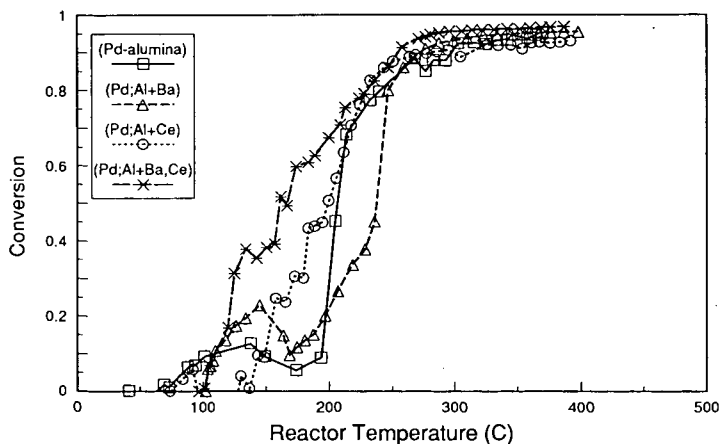


Figure 3.b: Effect of base metal additives on methanol conversion under stoichiometric feed conditions ($\lambda = 1$).

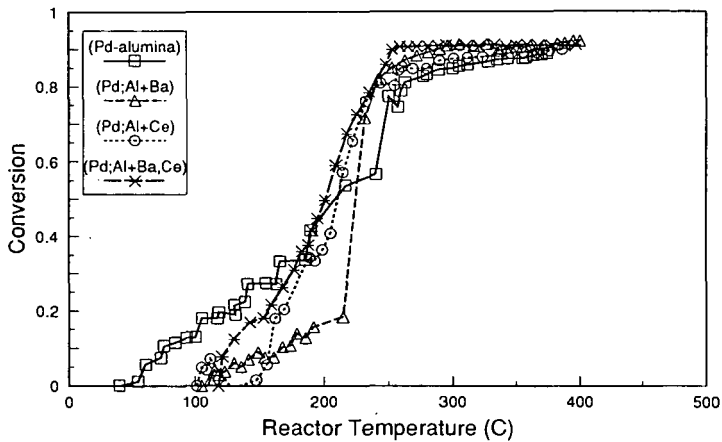


Figure 3.c: Effect of base metal additives on methanol conversion under lean feed conditions ($\lambda > 1$).

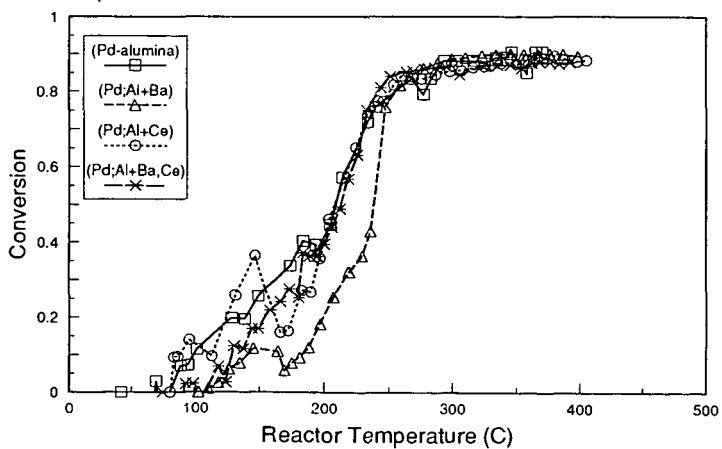


Figure 4: Effect of base metal additives on formaldehyde conversion under stoichiometric feed conditions ($\lambda = 1$).

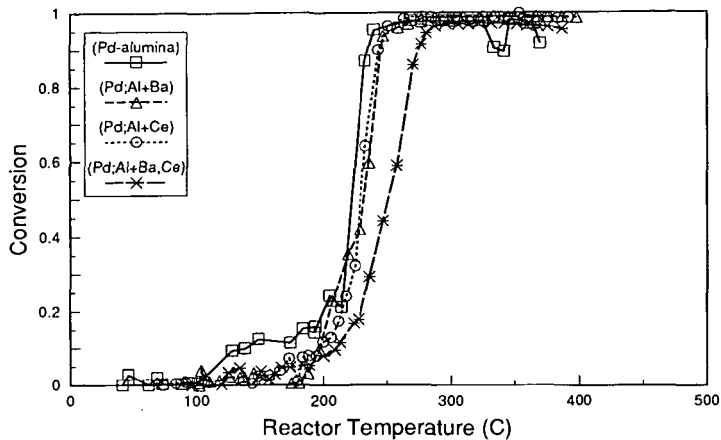


Figure 5: Effect of base metal additives on carbon monoxide conversion under stoichiometric conditions ($\lambda=1$).

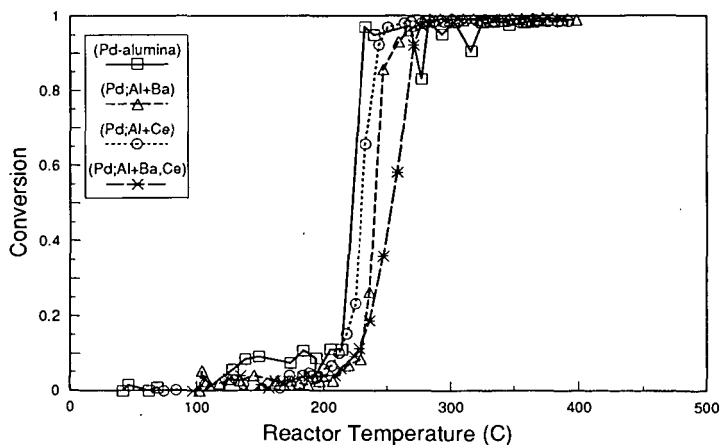


Figure 6: Effect of base metal additives on propylene conversion under stoichiometric conditions ($\lambda=1$).

OXIDATIVE COUPLING OF METHANE OVER
RARE-EARTH-BASED NONREDUCIBLE COMPOSITE-METAL-OXIDES CATALYSTS¹

Yuda Liu, Guodong Lin, Hongbin Zhang, Junxiu Cai,
Hiulin Wan, and K. R. Tsai
Department of Chemistry
Institute of Physical Chemistry
Xiamen University
Xiamen 361005, China

ABSTRACT

Nonreducible composite metal-oxides catalysts of the host-dopant type can be very effective catalysts for methane oxidative coupling (MOC) reaction(s) and for oxidative dehydrogenation of ethane to ethene. A systematic study of the relative efficacies of the alkali and alkaline-earth dopants used as selectivity promoters for lanthania-based MOC catalysts in relation to the cationic polarizabilities, and of the behavior of a CsOH-coated lanthania catalyst towards treatment with CO₂ plus O₂ near the MOC reaction temperature and toward CO₂-containing feeds has been made, together with laser Raman spectroscopic detection of superoxide ions in the freshly activated catalyst. The results strongly indicate that O₂⁻ adspecies is an active oxygen species responsible for the initial alkane-hydrogen-abstraction reactions.

INTRODUCTION

Methane oxidative coupling (MOC) over solid catalysts is of great current interest because of its potential importance in the utilization of the world's abundant natural gas resource for the production of ethylene or liquid fuels, and of its fundamental significance in the catalytic activation and selective conversion of the first and the most inert member of paraffin hydrocarbons. Much attention has been focused on the development of better catalysts for the MOC reaction(s) and on mechanistic studies of O₂ activation and methane conversion; and important advances have been made since the pioneering work of Keller & Bhasin [1], as shown by many recent reviews [2].

The great number of MOC catalysts reported in the literature may be roughly classified into three main categories (1) nonreducible composite metal-oxides with stable cationic valency; (2) basic-oxide-supported catalysts of reducible oxides of certain IVA, VA metals, e.g., PbO_x, Bi₂O_x, or oxides of certain IIb-elements (Zn and Cd); and (3) alkali-oxides (or phosphates or sulfates or chlorides)-promoted complex catalysts containing oxides of certain transition metals, e.g., MnO_x, TiO_x, MoO_x, and the recently reported CaO-NiO-K⁺ [3].

MOC catalysts of the first category are the most extensively investigated. These are usually of the host-dopant type, each consisting of a host oxide of a higher-valent cationic metal from the IIA or IIIB or IVB group doped with one or more basic oxides with lower and stable cationic valency from the IA, or IIA or IIIB group so as to generate or increase lattice anionic vacancies, which appear to be requisite for dioxygen chemisorption and activation. However, the IIA-IA

¹ Work supported by the National Natural Science Foundation of China and by a grant for spectroscopic characterization from the State Key Laboratory for Physical Chemistry of The Solid Surface, Xiamen University.

catalyst systems all suffer from the serious drawback of high volatilization loss of the alkali promoters and significant sintering at the MOC reaction temperature [2,3a]. The use of high-melting trivalent or quadri-valent metal oxides with stable cationic valency, such as alkaline-earth oxides (AEO) and/or oxides of IIIB metals, especially the M_2O_3 -type rare-earth-oxides (REO), many of which are known [4] to exist in the cubic C-type structure, a defective fluorite structure with regular disposition of anionic vacancies (e.g., Sm_2O_3). As pointed out in references [5-6], these REO with the C-type structure or layer-type structure (e.g., La_2O_3) are extremely open to oxygen chemisorption. These REO, especially Sm_2O_3 , have been found to show very high oxygen conversion efficiency and fairly good MOC activity and selectivity [2,7,8], but Sm_2O_3 appears to have only marginal C-type structural stability at the MOC reaction temperature [3a]. Doping La_2O_3 and Sm_2O_3 catalysts with small amounts of alkali or AEO has been found to enhance C_2 selectivity [2,3a,6-8], but the results from different investigators are not very consistent. It is known [9] that metal oxides with the fluorite structure (notably ThO_2) can form wide ranges of solid solutions with many M_2O_3 -type REO, and can also dissolve AEO to some extent, especially when the host-dopant cationic sizes are comparable. Thus defective-fluorite-structure (DFS) with high concentration of anionic vacancies can be created by proper doping of the fluorite-type host-oxides with metal-oxides of lower cationic valency. As recently shown by Cameron et al. [10], such dopings can radically change the low-activity ThO_2 host-oxide into very active and selective MOC catalysts for the co-feed operation. For the nonreducible composite metal-oxides, the active site for the initial alkane-hydrogen-abstraction reaction is most probably certain chemisorbed oxygen species, the very nature of which is still not clear, and remains a matter of controversy [2,6,10-12]. The mechanism of promoter action of the alkali and AEO dopants also remains to be clarified.

In this paper, further experimental evidence for the catalyst activities and selectivities in relation to structural types and anionic vacancies for this category of MOC catalysts is first presented; this is followed by presentation and discussion of the results of a systematic study of the relative efficacies of the alkali and AEO promoter in relation to the cationic polarizabilities, and of the behavior of a CsOH-coated La_2O_3 catalyst towards treatment by CO_2 plus O_2 , as well as towards CO_2 -containing feeds, together with detection of anionic-dioxygen species in the freshly activated catalyst, with the aim of shedding some light on the nature of the active oxygen species and the mechanism of the promoter action.

EXPERIMENTAL

Catalyst Preparation, Evaluation, and Characterization

Undoped La_2O_3 , Y_2O_3 , ZrO_2 , and ThO_2 , as well as the $[Y_2O_3]ZrO_2$ (35 mol.% Y:65 mol.% Zr), $[La_2O_3]ThO_2$ (30 mol.% La:70 mol.% Th), and $pSm_2O_3]ThO_2$ (30 mol.% Sm:70 mol.% Th) host-dopant pairs, the Bi_2O_3 -doped $[La_2O_3]ThO_2$ catalyst (10 mol.% Bi:20 mol.% La:70 mol.% Th), and the AEO-doped (5 mol.% M^{2+} in each case) La_2O_3 catalysts were prepared by drying and ignition (830-900°C, 1 hr) of freshly precipitated, or co-precipitated hydroxides, or carbonates in the case of the AEO-doped La_2O_3 catalysts, while the alkali-sulfates-doped La_2O_3 catalysts (5 mol.% M in each case) and the CsOH-coated lanthania catalyst (10 mol.% Cs:90 mol.% La) by impregnation of ignited lanthania with the aqueous metal sulfates and CsOH, respectively, followed by drying and ignition (700°C).

Catalyst evaluation was carried out in a quartz microreactor (6.0 mm i.d. with concentric quartz tubing serving as thermal-couple well)-G.C. (TCD) outfit, 0.20 mL of catalyst sample (30-60 mesh) being used in each case. The feed ($CH_4:O_2:N_2 = 24.6:5.6:69.8$ vol.% being used throughout this work) and the reactor effluents were analyzed with a gas chromatograph

(Shanghai Fenxi, Model #103) equipped with thermal conductivity detector, a molecular-sieve-5A column, as well as a Porapak-Q column, being used to separate O₂, N₂, CH₄, and CO, as well as CO₂, C₂H₄, and C₂H₆ (C₃₊ and H₂O being neglected), respectively, and N₂ as the internal reference for the quantitation of each gaseous component from its G.C. peak. The selectivity for each C-containing product and the ΣC₂ yield were expressed in terms of the carbon-efficiency (%) of methane conversion to the respective product. In each case, a 95 ± 2% carbon material balance was obtained. Laser Raman spectra for freshly activated sample of the CsOH-coated La₂O₃ catalyst and for partially deactivated sample, as well as for freshly prepared sample (ignited at 700°C for 1 hour in ambient air) before the activation treatment, were taken at room temperature with a Spex Ramalog-6 spectrometer with argon laser (5145 Å) as the excitation source.

RESULTS AND DISCUSSION

Catalyst Performance in Relation to Compositions and Structural Peculiarities

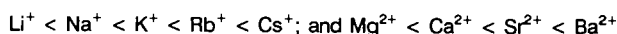
The experimental results show that doping ThO₂ with a trivalent-lanthanide oxide (La₂O₃ and Sm₂O₃ appeared to be equally effective), or ZrO₂ with Y₂O₃, to produce a composite metal oxide with defective fluorite structure (DFS) can be very effective in changing a poor MOC catalyst with no intrinsic anionic activity and, especially selectivity (Table 1), in accordance with observations by previous workers [10]. Note that these DFS metal-oxides are known to be solid electrolytes with high anionic conductivities, especially the zirconia-yttria system [9]. It is interesting to note that the 10 mol.% Bi₂O₃-doped [La₂O₃]ThO₂ catalyst appeared to be a highly efficient methane-combustion catalyst, rather than a MOC catalyst. Conceivably, the presence of the redox-active Bi (III/IV) in the DFS lattice of [La₂O₃]ThO₂ can promote the reductive dissociation of O₂ (O=O bond energy: 118 kcal) chemisorbed at an anionic vacancy into 2O⁻, most probably via the formation of O₂²⁻ (ionic 'O-O' bond energy: 34 kcal) as precursor; and high concentration and mobility of O⁻ in the catalyst may be conducive to deep oxidation of CH₄ (C₂H₆ and C₂H₄), and detrimental to MOC selectivity. Incidentally, doping a [25 mol.% LaO_{1.5}]ThO₂ with 5 mol.% PbO was also found to promote CO₂ formation (64% CO₂, 36% C₂).

Table 1
Catalyst Activity and Selectivity in Relation to Structural Peculiarities

Catalyst System Composition	Structure Type	Reaction Temp.(°C)	GHSV (h ⁻¹)	Conversion		Selectivity C ₂ (%)
				CH ₄ (%)	O ₂ (%)	
ThO ₂	Fluorite	760	12x10 ⁴	11	34	42
30 mol.% SmO _{1.5} -ThO ₂	DFS	760	12x10 ⁴	27	95	57
30 mol.% LaO _{1.5} -ThO ₂	DFS	760	12x10 ⁴	28	94	55
BiO _{1.5} -LaO _{1.5} -ThO ₂ (10 : 20 : 70)	DFS	700	12x10 ⁴	13	98	0 (100% CO ₂)
ZrO ₂	Monoclinic	760	3x10 ⁴	19	98	7
Y ₂ O ₃	C-type	760	3x10 ⁴	26	98	38
35 mol.% YO _{1.5} -ZrO ₂	DFS	760	3x10 ⁴	26	92	46

Promoter Effects of Alkali Sulfates and Alkaline-Earth Oxides on La₂O₃ Catalyst

The promoter effects were found to increase with increasing cationic sizes:



This may be correlated to the increasing tendencies towards the formation of the corresponding metal-superoxides [13-14], which, in turn, may be correlated to the increasing cationic polarizabilities [15]. Conceivably, by acquiring an electron trapped at an anionic vacancy, or from an O^{2-} ion, an O_2^- adspecies may be formed from a chemisorbed O_2 ; likewise, O_2^{2-} adspecies may then be formed by acquiring a second electron. The O_2^{2-} adspecies may dissociate reversibly into $2 O^-$, which may readily diffuse into the bulk. The half-life of anionic dioxygen adspecies, especially O_2^- , may be prolonged by side-on coordination [14] to a highly polarizable dopant cation (e.g., Cs^+ , Rb^+ , or K^+) known to have a strong tendency to form metal superoxide [12-13], which, however, is very sensitive to inhibition by moisture [14], due to conversion into the highly soluble and thermally very stable alkali hydroxide (with the exception of $LiOH$, which is barely soluble in water, and dehydrates to Li_2O at $850^\circ C$ [4b]). Note that the promoter effects of the alkali sulfates, with the notable exception of Li_2SO_4 , all appeared to decrease rapidly with time on stream. However, the promoter effect of Na_2SO_4 taken in the first 30 minutes to an hour was reproducibly found to be slightly better than that of Li_2SO_4 (Table 2).

Table 2
Promoter Effects of Alkali Sulfates and AEO on La_2O_3 -Based Catalysts

Catalyst (mol.%)	Temp. ($^\circ C$)	GHSV (h^{-1})	Conversion (%)		Selectivity (% Efficiency)		
			CH_4	O_2	C_2H_6	C_2H_4	ΣC_2
5% Li^+/La_2O_3	700	1.5×10^4	29.4	85.8	29.5	31.0	60.5
5% Na^+/La_2O_3	700	1.5×10^4	28	83	29	33	62
5% K^+/La_2O_3	700	1.5×10^4	29	80	30	35	65
5% Rb^+/La_2O_3	700	1.5×10^4	30	89	33	35	68
5% Cs^+/La_2O_3	700	1.5×10^4	29	80	34	36	70
La_2O_3	700	3.0×10^4	28.1	99.0	24.6	25.3	49.9
5% Mg^{2+}/La_2O_3	700	3.0×10^4	28.6	97.8	26.2	25.6	51.8
5% Ca^{2+}/La_2O_3	700	3.0×10^4	27.9	98.0	27.1	25.6	52.7
5% Sr^{2+}/La_2O_3	700	3.0×10^4	28.0	98.1	30.4	24.8	55.2
5% Ba^{2+}/La_2O_3	700	3.0×10^4	28.9	98.1	32.6	26.5	59.1

Effects of CO_2 Treatment and of CO_2 in Feed on $CsOH$ -Coated Lanthania Catalyst

The 10 mol.% $CsOH/La_2O_3$ catalyst was found to behave like molten $CsOH$ (ca. 25-30 Å thick) supported on La_2O_3 ($4 m^2/g$). The MOC activity and selectivity were again found to decline rapidly with time on stream (Table 3), most probably also due to inhibition by H_2O coproduced in the MOC reactions; but the ΣC_2 selectivity was increased with the addition of 4-5 vol.% of CO_2 into the feed, though with a slight depression in the CH_4 conversion. Moreover, the catalyst could be reactivated by treatment with CO_2 plus a few percents of O_2 . Laser Raman spectrum of the freshly activated sample taken at room temperature indicated the presence of a large amount of carbonate ($1086 cm^{-1}$ st, $700 cm^{-1}$ w), a small amount of CsO_2 ($1128 cm^{-1}$ w, plus some weak, unresolved and unidentified peaks around $980-1000 cm^{-1}$), the assignments of the Raman peaks being made with reference to [15-16]. After 3 hours on stream, only the large carbonate-peak at $1086 cm^{-1}$ remained; the peak assignable to CsO_2 being no longer visible. The spectroscopic characterization will be communicated in more details later. Conceivably, molten $CsOH$ can readily absorb CO_2 to form Cs_2CO_3 (d. $610^\circ C$ [4b]), which is readily decarbonated at $700^\circ C$ to form Cs_2O , which in turn can readily absorb O_2 to form, predominantly, CsO_2 [13], plus a small amount of Cs_2O_2 ; both of these may dissolve in the molten $CsOH$, and appear to be not so active and selective as compared with the previous case

of 5 mol.% Cs₂SO₄/La₂O₃ where O₂⁻ adspecies was probably partially stabilized by Cs⁺ dopant cations incorporated into the surface lattice of La₂O₃ during the impregnation and heat treatment.

Table 3
Effects of CO₂-O₂ Treatment and of CO₂ in the Feed on 10 mol.% CsOH/La₂O₃ Catalyst

Time (min.) on Stream	Feed or Reagent	Temp. (°C)	Conversion (%) ^a		Selectivity (%) ^a			YΣC ₂ ^a (%)
			CH ₄	O ₂	C ₂ H ₆	C ₂ H ₄	ΣC ₂	
0-30	Feed	700	27.8	94.7	30.1	23.9	54.0	15.0
30-150	Same	700	27.4	94.7	27.2	22.5	49.7	13.6
150-250	Same	700	26.4	95.8	26.5	21.9	48.4	12.8
250-310	CO ₂ +2% O ₂	700						
310-335	Feed	700	28.5	95.9	28.5	25.2	53.7	15.3
335-400	Feed+5% CO ₂	700	27.5	99.0	90.8	38.5	55.0	15.1
400-430	Feed	700	28.9	93.8	26.6	23.8	50.0	14.6
430-460	Feed+4% CO ₂	700	27.8	93.6	27.8	25.2	53.0	14.7

Feed: CH₄:O₂:N₂ = 24.6:5.6:69.8 (vol.%). GHSV: 2x10⁴h⁻¹. ^aData taken at the end of the time interval.

Thus the results of the last two sections strongly indicate that O₂⁻ adspecies, is an active-oxygen species responsible for the initial alkane-hydrogen-abstraction in the MOC reactions (and in oxidative dehydrogenation of ethane). This is in line with the known experimental fact that this step requires a fairly large activation energy [2.12a], and that significant amounts of O₂⁻ adspecies, rather than O⁻ and O₂²⁻ species, are present in the great majority of efficient MOC co-feed catalysts. These findings have important bearings on the design of MOC catalysts and operating conditions.

REFERENCES

- G. E. Keller and M. M. Bhasin, *J. Catal.*, **73** (1982) 9.
- (a) J. S. Lee and S. T. Oyama, *Catal. Rev.*, **30** (1988) 249; (b) G. J. Hutchings, M. S. Scurrall, and J. W. Woodhouse, *Chem. Soc. Rev.*, **18** (1989) 251; (c) Y. Amenomiya et al., *Catal. Rev.*, **32** (1990) 163; (d) J. H. Lunsford, *Catal. Today*, **6** (1990) 235; (e) J. H. Lunsford in "Natural Gas Conversion" (B. Delmon and J. T. Yates, eds.) p. 3, Elsevier, Amsterdam, 1991.
- P. Pereira, S. H. Lee, G. A. Somorjai, and H. Heinemann, *Catal. Lett.*, **6** (1990) 255.
- S. J. Korf, J. A. Ross, J. M. Diphooom, R. H. J. Veehof, J. G. van Ommen, and J. R. H. Ross, *Catal. Today*, **4** (1989) 27.
- (a) A. F. Wells, "Structural Inorganic Chemistry" (Oxford University Press, Oxford, 1984); (b) "CRC Handbook of Chemistry & Physics", 66th Ed., 91985).
- A. G. Anshits, E. N. Voskresenskaya, and L. I. Kurteeva, *Catal. Lett.*, **6** (1990) 67.
- J.-L. Dubois and C. J. Cameron, *Appl. Catal.*, **67** (1990) 49.
- K. Otsuka, Q. Liu, M. Hatano, and A. Morikawa, *Chem. Lett.*, (1987) 1835.
- J. M. DeBoy and R. F. Hicks, *J. Chem. Soc., Chem. Commun.*, (1988) 982.
- E. C. Subbarao (ed.), "Solid Electrolytes", pp 35-46) Plenum Press, 1980).
- J.-L. Dubois, B. Rebours, and C. J. Cameron, *Appl. Catal.*, **67** (1990) 73.
- Otsuka et al., *Chem. Lett.*, (1987) 77; *Inorg. Chim. Acta*, **121** (1986) 237.
- (a) E. Morales and J. H. Lunsford, *J. Catal.*, **118** (1989) 255; (b) Y. Osada et al., *Appl. Catal.*, **59** (1990) 59.

13. R. E. Hall in "Encyclopedia of Chemical Technology" (Kirk & Othmer, eds), 3rd Ed., vol. 17, pg 1, Wiley Interscience Press Inc., 1982.
14. V. H. Lux, R. Kuhn and T. Niedermaier, *Z. anorg. alleg. Chem.*, **298** (1959) 285.
15. L. Andrews, J.-T. Hwang and C. Trindle, *J. Phys. Chem.*, **77** (1973) 1065.
16. H. H. Eysel and S. Thym, *Z. anorg. alleg. Chem.*, **411** (1975) 97.